Lawrence Berkeley National Laboratory
LBL Publications

Title

Review on Interface and Interphase Issues in Sulfide Solid-State Electrolytes for All-Solid-State Li-Metal Batteries

Permalink
https://escholarship.org/uc/item/18j7p796

Journal
Electrochem, 2(3)

ISSN
2673-3293

Authors
Byeon, Young-Woon
Kim, Haegyeom

Publication Date
2021-09-01

DOI
10.3390/electrochem2030030

Copyright Information
This work is made available under the terms of a Creative Commons Attribution License, available at https://creativecommons.org/licenses/by/4.0/

Peer reviewed

eScholarship.org Powered by the California Digital Library
University of California

Review on Interface and Interphase Issues in Sulfide Solid-State Electrolytes for All-Solid-State Li-Metal Batteries

Young-Woon Byeon and Haegyeom Kim *

Materials Sciences Division, Lawrence Berkeley National Laboratory, Berkeley CA 94720, USA
*Correspondence: haegyumkim@lbl.gov; Tel.: +1-510-486-5137

Abstract: All-solid-state batteries have emerged as promising alternatives to conventional Li-ion batteries owing to their higher energy density and safety, which stem from their use of inorganic solid-state electrolytes instead of flammable organic liquid electrolytes. Among various candidates, sulfide solid-state electrolytes are particularly promising for the development of high-energy all-solid-state Li metal batteries because of their high ionic conductivity and deformability. However, a significant challenge remains as their inherent instability in contact with electrodes forms unstable interfaces and interphases, leading to degradation of the battery performance. In this review article, we provide an overview of the key issues for the interfaces and interphases of sulfide solid-state electrolyte systems as well as recent progress in understanding such interface and interphase formation and potential solutions to stabilize them. In addition, we provide perspectives on future research directions in this field.

Keywords: solid-state batteries; solid electrolyte; lithium metal; interface; interphase; stability

1. Introduction

For decades, rechargeable lithium-ion batteries (LIBs) using organic liquid electrolytes have been commercially used as a power source for portable electronic devices [1–3], and their use has recently expanded to mid–large-scale electrochemical energy storage applications, including electric vehicles (EVs) and grids [4,5]. For the success of EVs, battery technology must surpass the current limitation of driving ranges by achieving a larger capacity. According to a global technical goal for 2030, the specific energy of secondary batteries must reach 500 Wh kg^{-1}, which is much higher than the 246 Wh kg^{-1} of today's typical EV batteries used in the Tesla Model 3 [6–9]. To achieve such a high energy density, a Li-metal anode is considered to be an unrivaled component, owing mainly to its extremely high theoretical specific capacity (3860 mAh g^{-1}) and lowest reduction potential (−3.040 V vs. the standard hydrogen electrode). Safety issues have become more important than ever as battery sizes have increased. However, current LIB technology using liquid electrolytes cannot meet the requirements for the use of a Li-metal anode or safety [10,11].

In this respect, all-solid-state batteries (ASSBs), which use inorganic solid-state electrolytes (SSEs) instead of flammable organic liquid electrolytes, have emerged as promising alternatives to conventional LIBs. SSEs offer several advantages over conventional liquid electrolytes. First, ASSBs are stable even in extreme environmental conditions such as high pressure, temperature, overcharge, or external shock, and there is much less risk of ignition or explosion [12,13]. Second, it is believed that ASSBs can use a Li-metal anode since the sufficient stiffness of SSEs can mitigate the internal short circuit by suppressing the Li dendrite growth during the electrochemical cycles [14]. Third, the volumetric energy density can be improved by reducing its volume since there is no need to pack each cell and a simpler design through bipolar stacking is available for ASSBs [15,16]. Despite these advantages of ASSBs, important challenges remain to be addressed. Many SSEs display lower ionic conductivity at room temperature when compared to liquid electrolytes. Moreover, it is difficult to ensure the ion-transfer channel between the SSE and electrodes because of their unstable interfaces.

Of the various kinds of SSEs, sulfide SSEs have attracted significant attention due to their high ionic conductivity (10^{-2}–10^{-4} S cm^{-1}), which is comparable to that of organic liquid electrolytes [11,17,18]. Figure 1 summarizes the ionic conductivities of sulfide SSEs. Although the high ionic conductivity and deformability make sulfide compounds promising SSEs, several important challenges remain. Sulfide SSEs have an intrinsically narrow electrochemical stability window, which results in undesired (electro)chemical reactions between the sulfide SSE and electrodes during battery cycling [19], forming unstable interphases. Such interphase formation leads to operation failures of ASSBs. Therefore, considerable efforts are now focused on improving the interfacial stabilities between sulfide SSEs and electrode materials.

In this review, we present an overview of the limitations and recent achievements in the development of sulfide SSEs, with a particular focus on the stability issue of sulfide SSEs with lithium-metal anodes and various cathode active materials. We will not discuss the conductivities of sulfide SSEs, as this topic is already

well documented in previous review articles [11,20–23]. We further discuss recently proposed techniques to achieve a favorable interface between sulfide SSEs and electrodes in ASSBs. This review aims to provide not only a comprehensive description of the developments of sulfide SSEs but also insight into potential directions of future research.

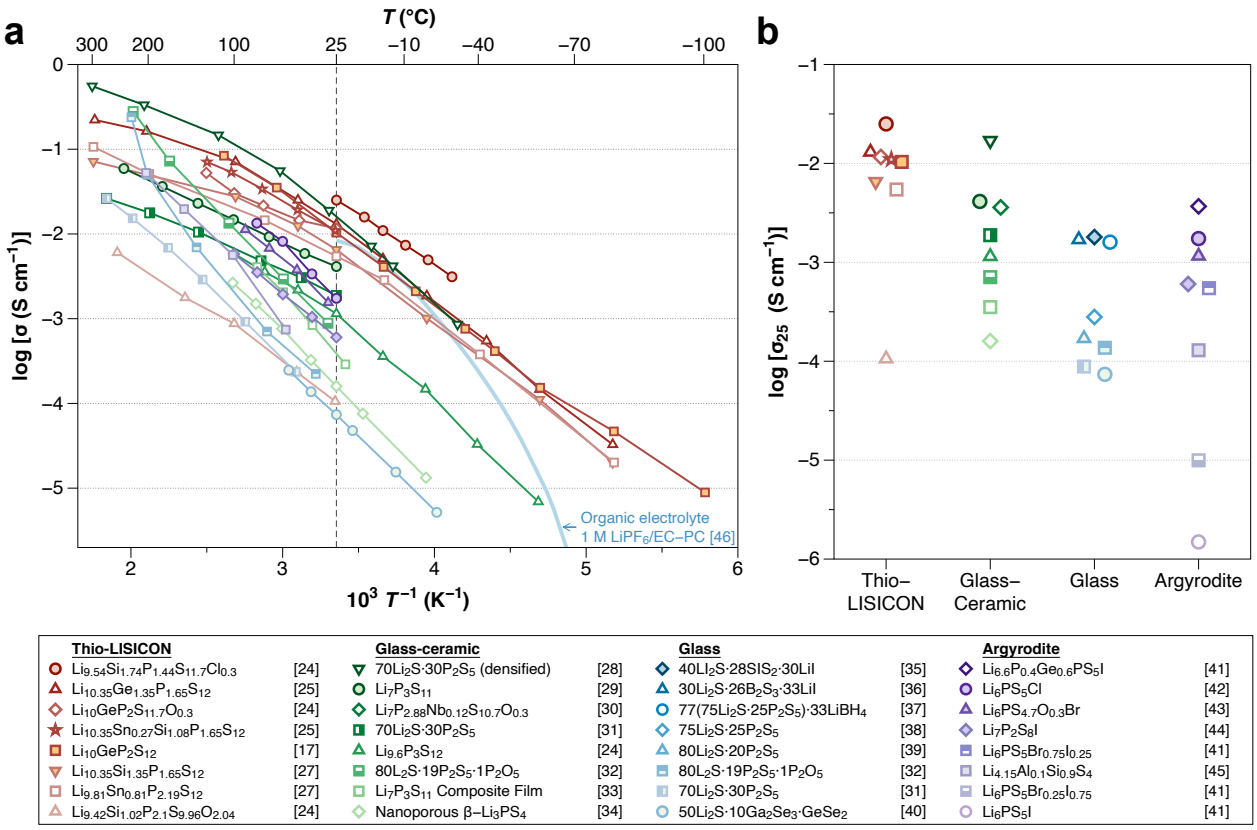

Figure 1. (**a**) Arrhenius-type plot of ionic conductivity for sulfide SSEs reported to date (as of February 2021). (**b**) The magnified view compares the conductivities at room temperature by their structure [17,24–45]. Note that the light blue line is a curve from organic liquid electrolytes of 1 M $LiPF_6$/EC-PC (50:50 vol%) for comparison [46].

2. Electrochemical Stability of Sulfide SSEs

The greatest challenge for sulfide SSEs is their very narrow electrochemical stability window, which leads to poor compatibility with electrodes. Although early works claimed that sulfide SSEs have a good electrochemical stability window of 0–4 V (vs. Li metal) based on cyclic voltammetry (CV) measurements [17,28,47], it is highly likely that these works overestimated their electrochemical stability. In the CV tests, the planar electrode geometry limits the contact area, leading to small currents, which can show kinetically extended electrochemical stability instead of a thermodynamic stability window. Later, Han et al. and Dewald et al. proved that the electrochemical stability windows of sulfide SSEs are indeed much narrower than those determined by previous CV tests [48,49]. To increase the 'active' contact area, they mixed $Li_{10}GeP_2S_{12}$ (LGPS) thiophosphate and carbon and measured the CV of the mixture, which presented a much lower

oxidation limit (<2.5 V vs. Li). In the mixture of LGPS–carbon, LGPS provides Li-transport pathways and carbon works for electron transfer. Therefore, such a configuration could show a 'practical' electrochemical stability window. This is critical since SSEs will encounter carbon additives in the cathode composite of ASSBs. Computational works have also demonstrated that sulfide SSEs have a narrow electrochemical stability window when compared with oxides and halides, as shown in Figure 2 [19,50,51]. Such a narrow electrochemical stability window is a major practical disadvantage of sulfide SSEs since the electrolyte must be stable over a wide range of lithium potentials between the anode chemical potential (0 eV/atom vs. Li) and the potential set by the cathode, which is near <−4.0 eV/atom for typical cathodes.

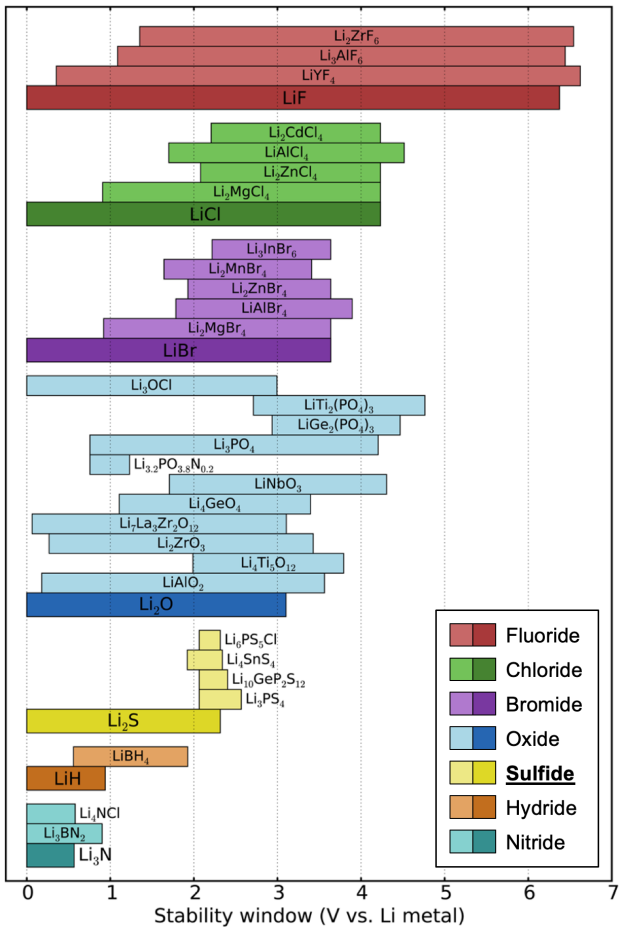

Figure 2. Theoretically driven electrochemical stability ranges of various electrolyte materials. Note that the yellow-colored sulfide electrolytes show low upper limits of less than 3.0 V. Reproduced with permission from reference [19], Copyright 2016 American Chemical Society.

3. Interfacial Stability

The narrow electrochemical stability window of sulfide SSEs leads to poor compatibility with both the anode and cathode. At the interface with electrodes, sulfide SSEs suffer from significant material degradation when electron-transport pathways are provided. Figure 3 summarizes the interfaces in sulfide-SSE-based ASSBs. With a Li metal anode, sulfide SSEs are reduced and form a solid-electrolyte interphase (SEI) layer

between the Li metal and SSE. Depending on the reduction products, the interface can be passivated or cause the continuous reduction of the SSE, thus leading to battery failure [19]. Another important issue at the anode side is dendritic Li growth during the charging of ASSBs. Although it was believed that rigid SSEs could prevent dendritic growth in the early stages of research, many reports have since shown Li dendritic growth and penetration through SSEs [52–55]. The situation is much more complicated on the cathode composite side. A cathode active material needs to be homogeneously mixed with an SSE and carbon to provide Li-ion and electron pathways. As a result, the cathode composite has more interfaces, namely cathode/SSE, carbon/SSE, and cathode/carbon. We will discuss recent findings of interfacial degradation mechanisms and approaches to overcome them in the following sections.

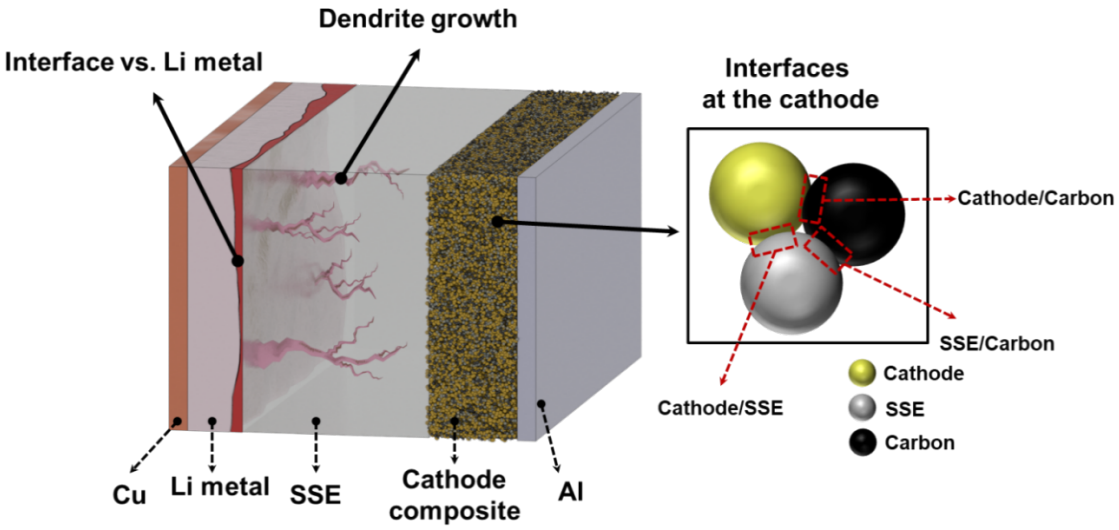

Figure 3. Schematics of interfaces and interphases in ASSBs.

3.1. Interface with Li-Metal Anode

Due to the inherently narrow electrochemical stability window, many sulfide SSEs decompose spontaneously simply by contacting a Li-metal anode [19]. Several efforts have been made to evaluate Li-metal/sulfide-SSE interfaces both theoretically and experimentally [18,50,56–67]. The interfaces formed between Li metal and the SSE can be classified into the following three types [68]. Type I interfaces are stable and ideal interfaces formed when the SSE does not react with Li metal electrochemically (Figure 4a). Most binary compounds, including Li_2S and Li_3P, form this 'type I' interface with Li metal. However, if the SSE is not electrochemically stable with Li metal, as most of the sulfide compounds are, the interphase will form at the interface as products of the SSE decompose. If the interphase material is highly conductive for both ionic and electronic transport, non-passivating interphases will form, and the reduction of SSE continuously occurs (Type II). Thus, the reaction front rapidly propagates into the SSE, leading to a short circuit and failure of the SSB (Figure 4b). When the interphases exhibit ionic conductivity but not electrical conductivity (Type III), the

interface becomes relatively stable (passivating interphase) because the decomposition reaction of the SSE is suppressed significantly (Figure 4c).

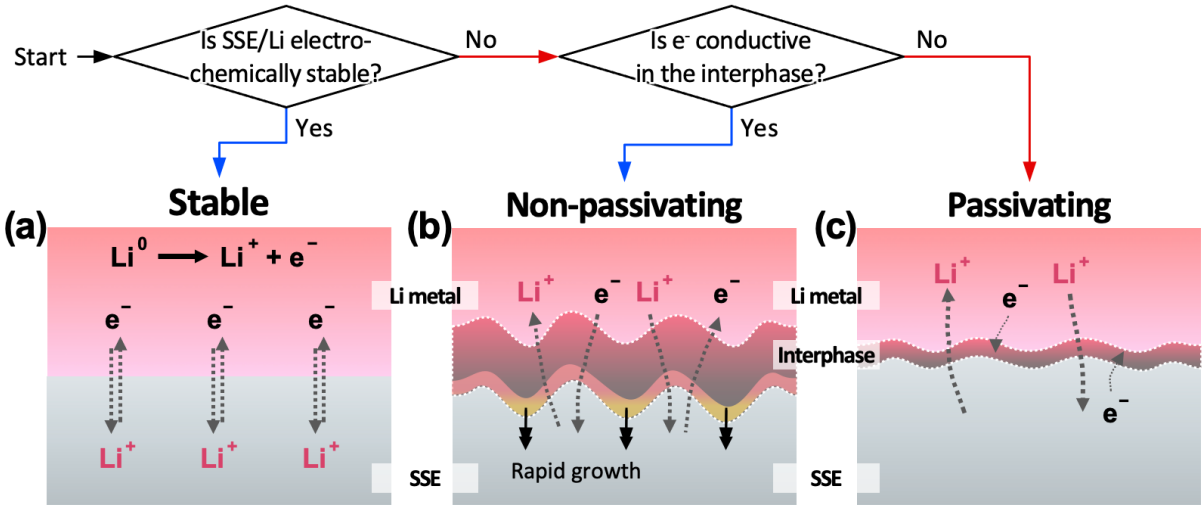

Figure 4. (**a**–**c**) Schematics of three different types of possible interfaces between SSE and Li-metal anode: (**a**) non-reactive and thermodynamically stable interface, (**b**) reactive and non-passivating interphase causing rapid and continuous decomposition of SSE, and (**c**) reactive but metastable passivating interphase that only conducts Li ions.

In situ X-ray photoelectron spectroscopy (XPS) measurements during Li vapor deposition of various sulfide SSEs by Wenzel et al. provide experimental evidence of the formation of passivating interphases [69–72]. For the crystalline $Li_7P_3S_{11}$ and Li_6PS_5X (X = Cl, Br, or I) argyrodites, Li_2S, Li_3P, and LiX (X = Cl, Br, or I) were formed at the interphase (Figure 5a), consistent with the theoretical predictions [73]. Despite the possible existence of the various reduced P phases in P 2p signals, the authors concluded that this reduced P phase likely originated from the reactions of Li_3P with residual oxygen and water in the UHV chamber. Some studies have pointed out that the oxygen (O) contamination in sulfide SSEs can lead to phase segregation in the lithium phosphate (Li_3PO_4) phase at the initial stage of the interphase formation reaction [74]. It remains debatable whether the oxygen-containing interphase formation should be attributed to the pre-existing oxygen in the sulfide SSEs or contamination from air exposure during the sample transfer. Correlative analysis from time-resolved electrochemical impedance spectroscopy (EIS) and XPS confirms that an increase in the thickness and resistivity of the interphase is gradually slowed down as more Li metal is deposited (Figure 5b) in the $Li_7P_3S_{11}$ system, suggesting that their interphase stabilizes the interface themselves (the formation of a passivating interphase). Similar passivating interphase formation has been reported in Li_6PS_5Cl (LPSCl) and Li_6PS_5Br [71].

In contrast to the passivating-layer formation of $Li_7P_3S_{11}$ and Li-argyrodite (Li_6PS_5Cl and Li_6PS_5Br)-related interphases, Li thiophosphates such as LGPS and LSPS ($Li_{10}SnP_2S_{12}$) are known to form a non-

passivating interphase upon contact with Li metal due to the presence of components (i.e., Ge^{4+} and Sn^{4+}) that provide electron-conducting pathways when reduced [71,75]. Wenzel et al. conducted in situ XPS experiments on LGPS material and reported its interfacial instability with Li metal [72]. Figure 5c shows the XPS spectra changes of LGPS before and after deposition of 31-nm Li metal. In addition to the formation of Li_3P and Li_2S, the reduction of Ge^{4+} to metallic Ge species is clearly detected and denoted as "reduced Ge" and "Ge metal or $Li_{15}Ge_4$" in Figure 5c. The fraction of Li_2S continues to increase even after 2 h (Figure 5d), indicating that the interfacial reaction is not yet finished at the end of the last deposition step and that the SEI is still growing (Figure 5e). Compared with that in germanium-free $Li_7P_3S_{11}$, the SEI formed in $Li_{10}GeP_2S_{12}$ grows much faster. It is interesting that the decomposition of LGPS continues given that the amount of Ge reduction measured in this study is much less than the amount of formed Li_3P and Li_2S. The authors attributed this to the formation of electronically conducting Ge phases that also have high Li diffusivity. Such non-passivating interphase formation leads to the high coulombic loss of LGPS, compared to LPS (specifically, $Li_{9.6}P_3S_{12}$), as shown in Figure 5f [24].

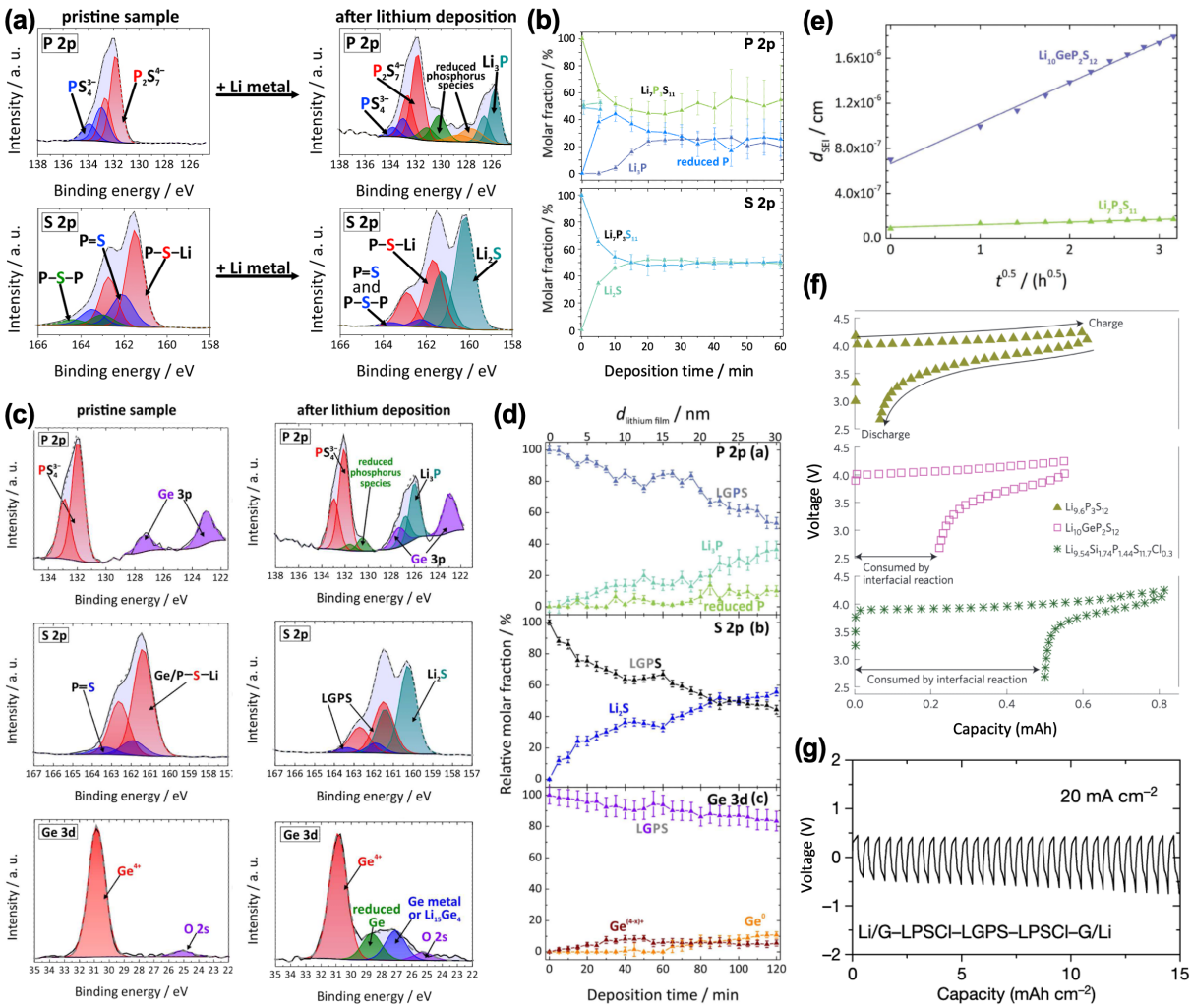

Figure 5. (**a**) Modeled XPS detail spectra for the S 2p and P 2p signals before and after 80 min of Li deposition on the $Li_7P_3S_{11}$ SSE ceramic. (**b**) Time-dependent molar fraction change curves of

phosphorous and sulfur species of $Li_7P_3S_{11}$, showing the evolutions of the decomposition products, namely Li_3P, reduced P species, and Li_2S, reprinted from reference [70], Copyright 2016, with permission from Elsevier. (**c**) XPS detail spectra and peak fits of pristine LGPS (left) and that reacted with Li metal (right) for the P 2p, S 2p, and Ge 3d signals. (**d**) Profiles of the decomposition products for the phosphorous, sulfur, and germanium species measured during the lithiation of LGPS as a function of Li deposition time. (**e**) Dependence of SEI thickness on the square root of time, adapted with permission from reference [72]. Copyright 2016 American Chemical Society. (**f**) Electrochemical stability of the LPS/LGPS family, reproduced with permission from reference [24]. Copyright 2016 Springer Nature. (**g**) high-rate test (20 mA cm^{-2}, at 55 °C) for the cell with configuration of LPSCl–LGPS–LPSCl as SSE and graphite-covered lithium (Li/G) as the electrodes, reproduced with permission from reference [76]. Copyright 2021 Springer Nature.

Various solutions have been reported to engineer the compatibility between SSEs and Li metals. For example, Yang et al. suggested antiperovskite lithium oxychloride, Li_3OCl, as a potential artificial passivating compound to stabilize the interface between SSEs and Li metal [77]. As also well predicted in Figure 2 (located at the top of the oxides) [19], antiperovskites are theoretically stable at 0 V, owing to the absence of reducible non-Li cations in the composition [10]. In their experiments, Li-symmetric cell shows a stable voltage polarization profile >100 h at 0.035 mA cm^{-2}. However, their approach did not expand on how to incorporate their artificial passivating compound into the full cell systems. Recently, Ye et al. proposed an interesting solution for the poor interfacial stability of sulfide SSEs with Li metal [76]. For example, the Li–LGPS–Li symmetric cell exhibited very poor cyclability at 0.25 mA cm^{-2} (corresponding to 0.5C), with a voltage spark after 3 cycles. Even for LPSCl, which is well known for being more electrochemically stable, a short-circuit occurred after over 150 h of operation under the same test condition. However, by employing combined strategies of multilayer stacking of the electrolytes, a less-stable electrolyte sandwiched between more-stable SSEs, and covering of the Li-metal anode with a graphite film, the authors demonstrate superior cycling performance for 1800 h under the same condition (0.25 mA^{-2}) without any observable voltage drops for the Li/G–LPSCl–LGPS-LPSCl–G/Li symmetric cell. Further, this cell is also stable for up to 15 h of operation at 20 mA cm^{-2} (corresponding to 40C, Figure 5g). The authors suggested that the multilayer design can prevent lithium dendrite penetration because the decomposition products of SSEs at the interface between LGPS and LPSCl fill and heal cracks. However, this mechanism has not yet been fully proven.

Recently, operando XPS (opXPS) measurements were developed and applied to investigate a Li/Li_2S–P_2S_5 interface by Wood et al. This technique mimics the charging–discharging process of a battery system using an electron gun (for lithium plating, charging) and ultraviolet-light source (for lithium stripping, discharging) [74]. Figure 6a presents schematics of the operando XPS technique employed in this study. By following the general trends in the phase-composition changes during charge/discharge half-cycles (Figure 6b),

the opXPS profiles having depth information of the interphase reveal that the interphase has a layered configuration composed of $Li^0/Li_2O/Li_3P/Li_2S/LPS$ (Figure 5c). The authors claim that Li_2S and Li_3P phases form first on the LPS, followed by Li_2O phase formation, and finally Li^0 deposition. The authors argued that Li_2O converts into Li_2O_2 and that Li_3P transforms into the Li-deficient phase $Li_{3-x}P$ via delithiation during discharging (lithium-stripping process), as shown in Figure 6d, since Li_2O and Li_3P are the redox-active species.

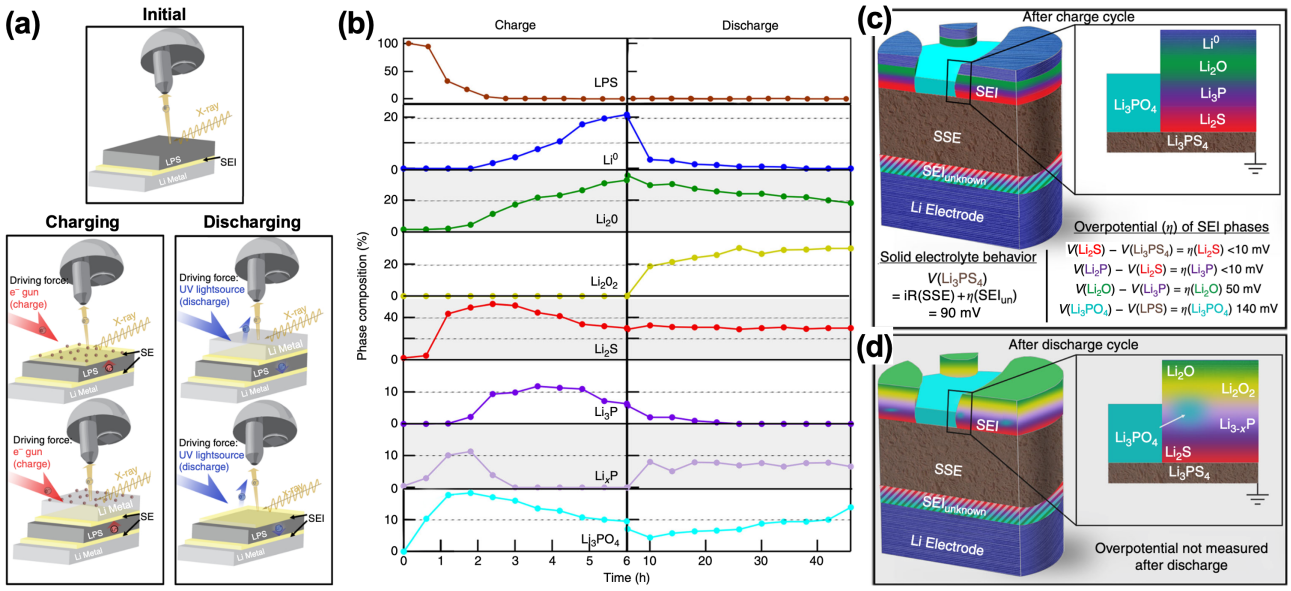

Figure 6. (**a**) Schematics of opXPS technique employed in the study. (**b**) Evolution of SEI phase composition as a function of time for both the charge and discharge half-cycles, clearly showing the redox activity of the Li_2O and Li_3P components of the interphase during the discharge half-cycle. (**c**,**d**) Summary of SEI composition and morphology after (**c**) charge and (**d**) discharge step. All the figures are adopted from reference [74] with permission. Copyright 2018 Wood, K. N et al. under the Creative Commons CC BY license.

3.2. Li-Dendrite Penetration

Dendritic Li growth and its penetration through SSEs is a major issue that must be addressed for the commercialization of ASSBs. In general, Li dendrites grow at relatively high current rates even in SSE systems, and the dendrites lead to a short circuit of the battery cell. In addition, the Li dendrite will form a new interface once it penetrates a SSE, and then, it will decompose the SSE and form a SEI layer, which will lead to deterioration of the battery performance. For example, $0.75Li_2S–0.25P_2S_5$ glass electrolyte shows a voltage drop in a Li-symmetric cell when the current is larger than 0.4 mA cm^{-2}; this voltage drop indicates the short circuit of the cell [78]. Similarly, other sulfide SSEs have relatively low critical currents (<1.5 mA cm^{-2}) that result in short circuits [79–81], which are much lower critical currents than those for liquid electrolytes (>10 mA cm^{-2}) [82] A very recent work by Otoyama et al. confirmed that Li metal can penetrate through the Li_3PS_4 SSE using in situ X-ray computed tomography (X-ray CT) [83]. Figure 7a presents the

galvanostatic cycling results of the Li/Li_3PS_4/Li symmetric cell under three different current rates of 0.24, 0.40, and 0.80 mA cm^{-2}. Tomograms in the XY, YZ, and ZX planes were obtained from the X-ray CT measurements (Figure 7b). The authors claimed that a crack is formed when Li_3PS_4 is decomposed in contact with Li metal since the volume expanded. Then, Li metal could easily penetrate the cracks and form new interfaces of Li/Li_3PS_4. Such a reduction–expansion–cracking reaction is repeated and thus makes large cracks and form Li clusters inside the Li_3PS_4 electrolyte, finally causing a short circuit (Figure 7c,d). A very recent study by Ning et al. using in situ X-ray CT in Li/Li_6PS_5Cl/Li system also demonstrated that the cracking is initiated near the surface with the plated electrode, and that the cracks propagate across the electrolyte from the plated to the stripped electrode [84], which agrees well with previous observations [83]. Similarly, Kazyak et al. observed Li dendrite penetration through Li_3PS_4 electrolyte using operando optical microscopy [54].

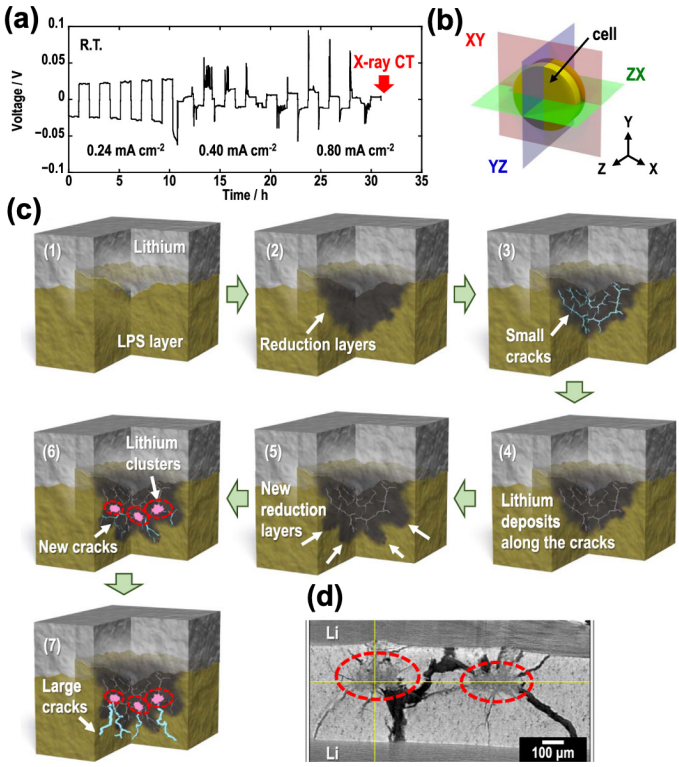

Figure 7. (**a**) Galvanostatic cycling test of Li/LPS/Li cell at room temperature. (**b**) Schematic diagram of the cell. (**c**) Crack formation mechanism initiated at the interface between the lithium and LPS pellet. (**d**) Tomogram of the Li/LPS/Li cell after short-circuiting, where the red circles indicate low density areas (e.g., lithium clusters), reprinted with permission from reference [83]. Copyright 2021 American Chemical Society.

It is widely known that Li dendrite grows even in SSEs. However, it remains unclear how Li dendrite can penetrate through inorganic SSEs. Some plausible scenarios have been suggested (Figure 8a). First, Han et al. proposed that the relatively high electronic conductivity of SSEs is the origin of Li-dendrite formation within the electrolyte after monitoring the dynamic evolution of Li concentration profiles in SSEs during Li-metal plating using time-resolved operando neutron depth profiling (Figure 8b–d) [85]. They quantified the net

amount of Li transported and compared it with the cumulative electric charge (Figure 8c,d). In the LiPON system, they did not observe a noticeable difference between the total amount of Li transported and the cumulative charge (Figure 8c). In contrast, a smaller amount of accumulated Li is observed than the cumulative charge in the Li_3PS_4 system (Figure 8d). Thus, they suggested that the Li dendrites are formed in the deep and undetectable region of the SSEs. Similar behavior is also observed in the LLZO electrolyte system. Given that the electronic conductivities of LLZO (10^{-9} S cm^{-1}) and Li_3PS_4 (10^{-8} S cm^{-1}) are much higher than that of LiPON (10^{-15}–10^{-12} S cm^{-1}) [86–88], they concluded that the relatively high electronic conductivity results in the Li dendrite formation. Second, in a recent work by Bruce's group, it was proposed that voids formed during stripping increase the 'effective' current significantly because of the poor contact between Li metal and SSEs, thereby resulting in the dendritic formation upon plating in the Li_6PS_5Cl electrolyte system [89]. Figure 8e summarizes the proposed mechanism of Li-dendrite formation. The authors claimed that the high stacking pressure of the ASSBs can overcome the Li-dendrite growth issue: the Li-symmetric cell with 7 MPa did not show a noticeable polarization increase during 100 cycles at 1.0 mA cm^{-2}, whereas the cell with 3 MPa showed a substantial increase of polarization during stripping and short circuit after 8 cycles at the same current density. A high stacking pressure forms more uniform interface between a SSE and Li metal, thereby increases contact areas. Thus, higher current density is needed to make Li dendrite penetration through the SSE at high stacking pressures. In a very recent computational work, void formation in Li metal during stripping was shown to depend on the lithiophilicity of the interface [90]. For example, Li_2O and LiPON have lithiophilic interfaces with Li metal and do not show accumulated voids at the interface during the striping process in their density functional theory (DFT) and kinetic Monte Carlo (KMC) computations. In contrast, LiF with lithiophobicity shows accumulated void formation at the LiF/Li interface. This finding suggests that interface and coating design play important roles in suppressing Li dendrite growth. Third, it was proposed that the relatively high stacking pressure in ASSBs accelerates Li penetration through the SSEs [91–93]. Although some degree of stack pressure is required to ensure contact between an SSE and Li-metal anode [94], too high of a stack pressure results in Li dendrite penetration through the SSE and thus a short circuit. Recently, Meng's group investigated the effect of stack pressure of ASSBs on the short-circuit behavior using the pressure-monitoring system shown in Figure 8f [91]. They observed the charge/discharge profiles of Li/Li_6PS_5Cl/Li symmetric cells at 75 μA cm^{-2} with different stack pressures from 5 to 75 MPa (Figure 8g). Interestingly, the cell with a very high stack pressure of 75 MPa showed a short circuit even before the Li plating and stripping test was conducted. The authors claimed that the short circuit at such high stack pressure is due to the creeping of Li metal to flow within the pores of Li_6PS_5Cl. When the stack pressure was lowered, the cell ran longer before the short circuit occurs. For example, for the cell with a stack pressure of 5 MPa, a short circuit was not observed within 1000 h of plating and stripping. In a full-cell configuration, the cell with a stack pressure of 5 MPa showed no short-circuit behavior and a typical charge–discharge

profile, delivering a specific capacity of 150 mAh g^{-1} (Figure 8h). In contrast, the cell was short-circuited when the pressure was increased to 25 MPa. Large low-density structures were also observed in the SSE using X-ray tomography after the electrochemical Li plating and stripping process at 20 MPa. It was speculated that these low-density structures are Li dendrites and SEI formed between Li metal and Li_6PS_5Cl. Based on their observations, it is clear that the stack pressure is an important parameter to control Li plating and stripping behavior in ASSB systems; this idea is also supported by a recent work by Hänsel et al. [93]. In their work, they investigated the effect of the thickness of Li_6PS_5Cl at no current condition and observed that the time required for short circuit monotonically increases with the thickness of the Li_6PS_5Cl SSE. This finding demonstrates that the short circuit at high stack pressure occurs via Li extrusion through the micropores of SSEs. The same group also discovered that the characteristics of SEI affect Li and Na exclusion, and thus short-circuit behaviors, considerably [92]. In their comparison study, they showed very sharp contrast between Li_3PS_4/Li and Na_3PS_4/Na systems: Li_3PS_4 showed short circuit at 45 MPa after 55 h, whereas Na_3PS_4 did not show such behavior at the same stack pressure even after 250 h. The authors claimed that the root cause of these contrasting observations is the different characteristics of the SEI formed between Li_3PS_4 and Li metal vs. Na_3PS_4 and Na metal. Whereas the Li_3PS_4/Li system forms a very thin passivating layer, the SEI continues to grow at the Na_3PS_4/Na interface because of the relatively high electronic conductivity of Na_3P and Na_2S compared to that of their Li counterparts, confirmed by the density of states (DOS) computations. These results indicate that the thickness and mechanical properties of the SEI formed between an SSE and Li-metal anode are crucial parameters to enable the realization of Li-metal ASSBs.

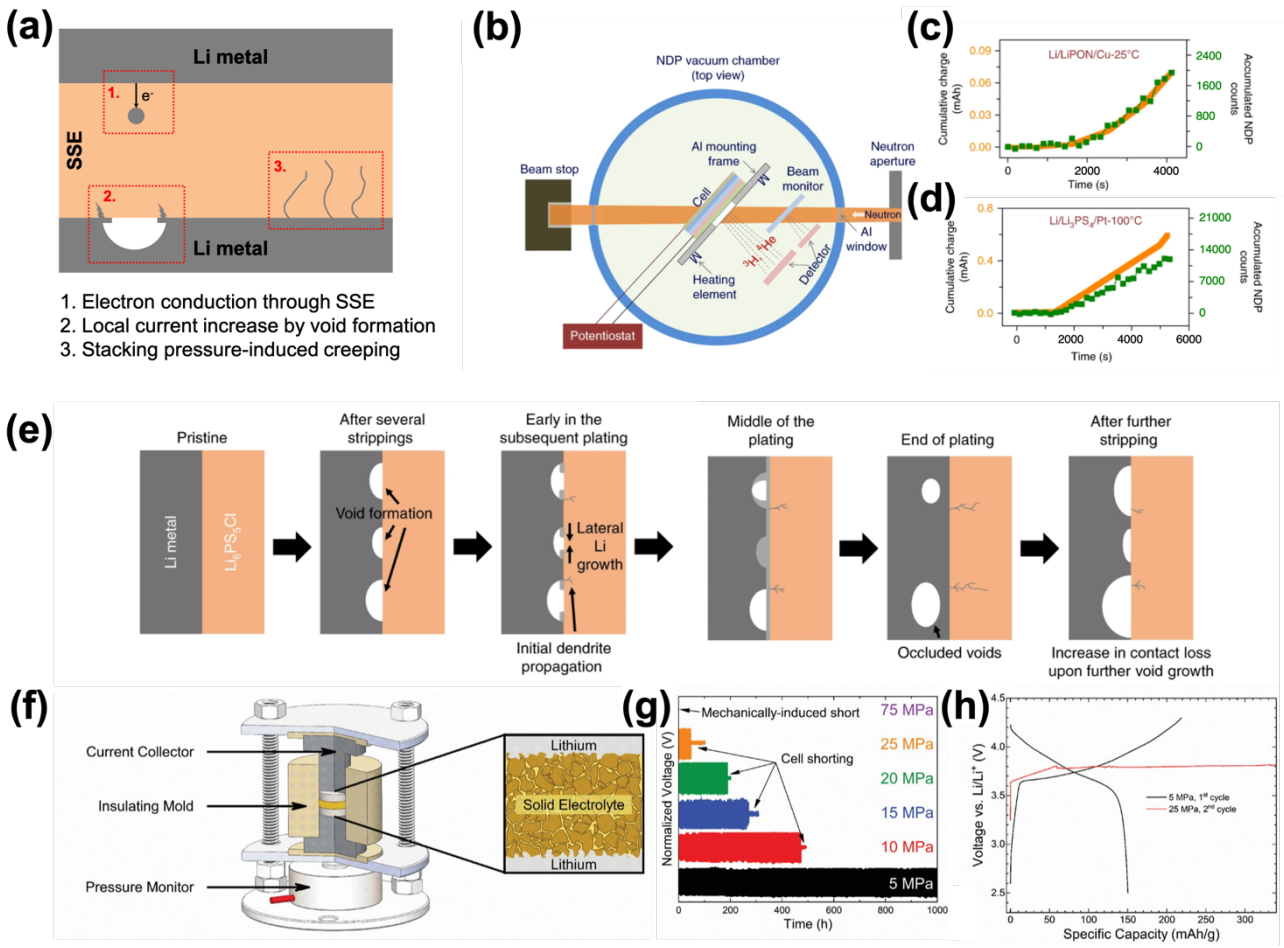

Figure 8. (**a**) Schematic showing the possible scenarios of Li dendrite penetration into SSE. (**b**) Schematic of the experimental set-up for operando NDP conducted in [85]. (**c**,**d**) Correlation between NDP counts (green dots) and accumulated charge (orange line) in the total region of (**c**) $LiCoO_2$/LiPON/Cu cell and (**d**) Li/LLZO/Cu cells tested at 100 °C, reproduced with permission from reference [85]. Copyright 2019 Springer Nature. (**e**) Schematic of Li metal/Li_6PS_5Cl interface cycled at an overall current density above the critical current for stripping, reproduced with permission from reference [89]. Copyright 2019 Springer Nature. (**f**) Schematic showing the design of the solid-state Li symmetric cell, allowing control and monitoring of pressure during cycling. (**g**) Normalized voltage of the cell as a function of time. (**h**) Voltage profile of a full cell using Li-metal anode with different stacking pressure. Figure f–h are adopted from reference [91] with permission. Copyright 2019 Wiley-VCH.

3.3. Interface with Cathodes

The cathode side has complicated interfaces since it contains various components to provide both electron and ion-conduction pathways. Typically, the cathode composite consists of a cathode active material, electron-conducting carbon, and an ion-conducting SSE. Therefore, it forms three distinct interfaces, cathode/carbon, cathode/SSE, and carbon/SSE (as shown in Figure 3). At the early stage of sulfide SSE development, sulfide SSEs were thought to be stable upon electrochemical oxidation [17,28,47]. However, recent works have

shown that most of the sulfide SSEs are prone to instability during oxidation when electron pathways are provided [48,49,95–98]. Specifically, Zhang et al. investigated the interfacial properties of a carbon-containing cathode composite with a LGPS SSE [96]. Figure 9a presents a schematic illustration showing how the electron-conducting carbon additives affect the electrochemical reaction processes at the $LiCoO_2$/LGPS interface. They found that the carbon additive contributes to an additional slope during the charging process and degrades the LGPS electrolyte, which increases the overpotential and thus decreases the specific capacity. In their ex situ XPS characterizations, it was confirmed that the $LiCoO_2$/LGPS cathode composite with carbon additive shows much more pronounced decomposition of LGPS and produces more insulating sulfide products than the composite without carbon after 100 cycles. In addition, as shown in Figure 9b, the cathode composite without carbon additive exhibits better cycling stability after 100 cycles at 115 μA cm^{-2} (0.1C). Yoon et al. also demonstrated similar degradation mechanisms at the interface between LGPS and carbon [95]. Both groups observed that the degradation of the LGPS/carbon interface does not depend on the structure and morphology of the carbon additives. It is a great challenge because the sulfide SSE will decompose once electron pathways are provided, which is essential to enable ASSBs. However, we expect that it is possible to slow down such degradations by using a low carbon content or low surface area of carbon.

Chemical and electrochemical degradation of sulfide SSEs at the interface with the cathode material is another important hurdle to overcome. Sakuda et al. observed the interfacial layer between a $LiCoO_2$ cathode and Li_2S–P_2S_5 sulfide-SSE after the first charging using TEM and EDS, as shown in Figure 9c [99]. The authors reported the mutual diffusions of Co, P, and S at the interface between the $LiCoO_2$ cathode and sulfide SSE. The formation of the interfacial layer increases the resistance of the cell significantly. In contrast, the authors were able to suppress the mutual diffusion and the formation of the interfacial layer by coating a Li_2SiO_3 thin film on the $LiCoO_2$ cathode particle, thereby improving the specific capacity. Similarly, the diffusion of S, P, and Cl into $LiNi_{0.8}Co_{0.1}Mn_{0.1}O_2$ cathode particle was confirmed by the SEM/EDS technique [100]. Later, Walther et al. further studied the degradation mechanisms of the cathode composite of Li_6PS_5Cl/$LiNi_{0.6}Co_{0.2}Mn_{0.2}O_2$ [101]. They characterized the interphase formation using XPS combined with time-of-flight secondary-ion mass spectrometry (ToF-SIMS) to determine the composition and microstructure of interphases. Phosphate and sulfate compounds were detected by their ex situ XPS analysis after 100 cycles, which agrees with a report by Visbal et al. [102,103]. ToF-SIMS obtains compositional and morphological information on the interphases beyond the capability of XPS. To investigate the spatial fragment distribution, the depth profiles were reconstructed, as shown in Figure 9d. The results show that the intensities of the phosphates and sulfates are dominated by the interface regions, demonstrating the formation of the SEI with PO_x and SO_x enriched. In the investigation of the interphase formation between the Li_6PS_5Cl SSE and $LiMn_2O_4$ cathode by Auvergniot et al., it was observed that the Li_6PS_5Cl electrolyte decomposes upon electrochemical cycling by scanning Auger microscopy (SAM) analysis. Figure 9e and f present the SAM

mapping results before and after cycling, respectively. Before the electrochemical cycling, the S and Cl signals overlapped. However, the S-rich and Cl-rich regions are clearly separated after 22 cycles. The authors also observed such SSE decomposition and SEI formation in other oxide cathode systems, including $LiCoO_2$ and $LiNi_{1/3}Co_{1/3}Mn_{1/3}O_2$ [103].

A recent study by Li's group presented interesting experimental results that the oxidation stability of a sulfide SSE, LGPS, can be improved significantly and that the oxidation stability window can be expanded up to 10 V vs. Li metal by high mechanical stack pressure even if conductive carbon (10 wt%) is added [104]. The authors claimed that the high mechanical constriction can kinetically stabilize sulfide SSEs based on their DFT computations and experimental observations. Note that the authors used graphite-film-covered Li metal to avoid Li metal penetration through the LGPS electrolyte at high stack pressure. They presented good cycling stability: 91% retention after 360 cycles in $LiCoO_2$/LGPS/$Li_4Ti_5O_{12}$ and 82% retention after 100 cycles in $LiNi_{0.5}Mn_{1.5}O_4$/LGPS/$Li_4Ti_5O_{12}$ full-cell configurations. In ex situ XPS characterizations, no significant decomposition reactions of LGPS were observed. The effects of mechanical constriction on the electrochemical stability window of sulfide SSEs are well summarized in a recent review article [105]. However, it is questionable if such a high stack pressure (>250 MPa) of the cell is practically feasible and how much the cost of manufacturing ASSBs would increase.

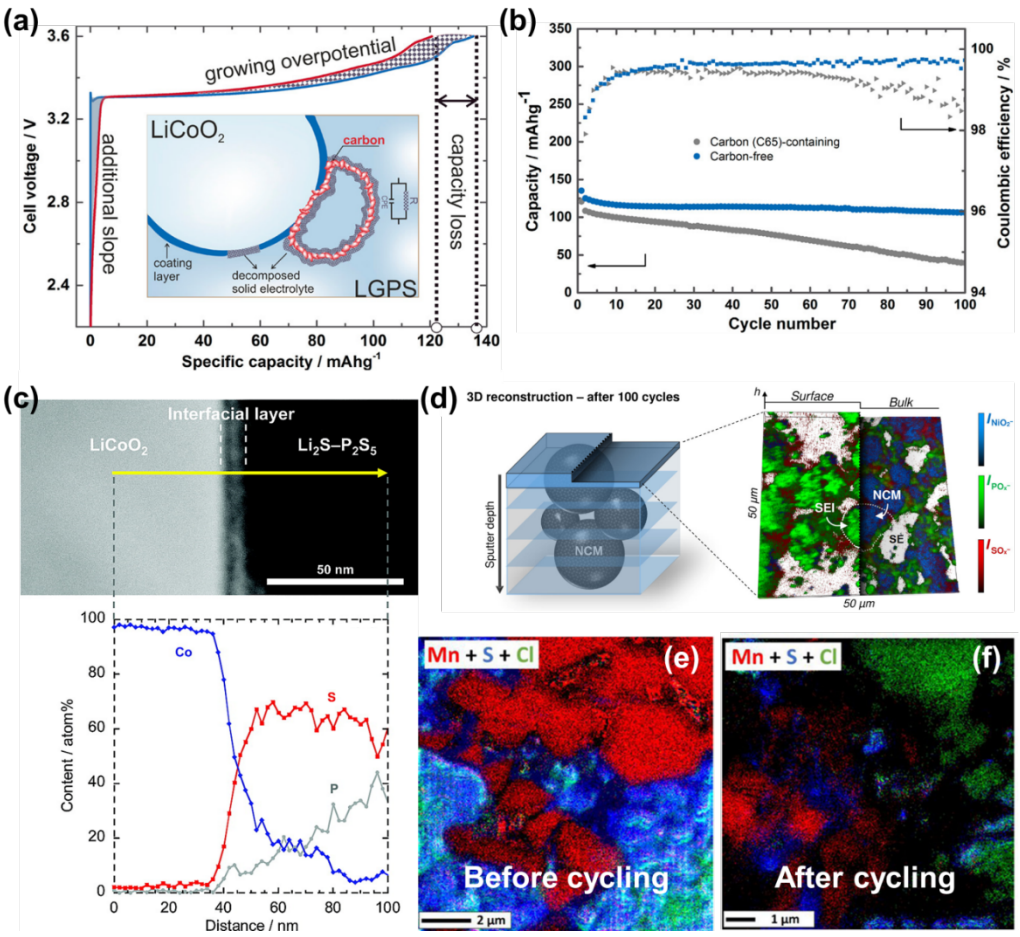

Figure 9. (**a**) Direct comparison of the first charge curves with (red)/without (blue) carbon additives in SSBs and a schematic showing the situations at the cathode/SE interface of the SSB during charge (Li insertion) processes. (**b**) Cycle performance of model SSBs with (grey)/without (blue) carbon additives, reprinted with permission from reference [96]. Copyright 2017 American Chemical Society. (**c**) Cross-sectional HAADF-STEM image of $LiCoO_2/Li_2S–P_2S_5$ solid-electrolyte interface after initial charging and corresponding EDX elemental line profiles, reprinted with permission from reference [99]. Copyright 2010 American Chemical Society. (**d**) Schematics showing the process of three-dimensional reconstruction of the depth profile of the cycled composite cathode, reprinted with permission from reference [101]. Copyright 2019 American Chemical Society. (**e**,**f**) Scanning Auger microscopy mapping of the composite LMO electrode of the LMO/Li_6PS_5Cl/Li–In half-cell before/after cycling, reprinted with permission from reference [103]. Copyright 2017 American Chemical Society.

A representative strategy to avoid (electro)chemical degradation of the interface between a cathode and a sulfide SSE is the 'cathode coating' approach. Many ternary-metal oxide compounds have been studied for use as cathode coatings, including $LiNbO_3$, $LiTaO_3$, $Li_4Ti_5O_{12}$, Li_2SiO_3, $LiAlO_2$, $Li_2CoTi_3O_8$, and Li_2ZrO_3 [24,56,99,106–114]. In theory, cathode coatings can separate an SSE from the low Li chemical potentials of the cathode in its highly charged state and prevent electrochemical self-decomposition of the SSE. However, such oxide coating compounds could not solve the interfacial issue between the cathode and sulfide SSE completely. In many cases, S/O exchange between coating materials and sulfide SSEs occurs, driven by the strong binding energy of PO_4 groups, as confirmed by computational studies [51,115]. Recently, Zhang et al. observed a sharp contrast between two coating materials, Li_2ZrO_3 and $Li_3B_{11}O_{18}$ [116]. They show that Li extraction occurs at Li_2ZrO_3 during the first charge process and that it loses its protection capability for the cathode. It was also observed that metal sulfides form within the Li_2ZrO_3 coating after 50 cycles. Therefore, it presents ~60% capacity retention after 100 cycles (Figure 10a). In contrast, $Li_3B_{11}O_{18}$ coating material shows much improved cycling stability, ~80% retention after 100 cycles. The $Li_3B_{11}O_{18}$ coating is also confirmed to be well maintained even after 10 cycles using STEM, as shown in Figure 10b,c.

Yihan et al. conducted a computational investigation to identify Li-containing cathode coating materials [115]. In their work, the phase stability, electrochemical and chemical stability against both cathodes and SSEs, and ionic conductivity were considered. The computational screening identifies polyanionic oxide compounds as promising cathode coating materials, including phosphates and borates. Figure 10d shows the electrochemical stability windows of six polyanionic oxides selected by Yihan et al. For better comparison, they plotted the electrochemical stability windows of common sulfide SSEs: Li_6PS_5Cl (LPSCl), LGPS, the glass-ceramic LPS, garnet-type LLZO, and ternary non-polyanionic coating materials such as Li_2ZrO_3, $LiNbO_3$, and $LiTaO_3$. Polyanionic oxides have much higher oxidation stability (>4.5 V) than non-polyanionic oxides (3–4 V). They explained that the higher oxidation limit of polyanionic oxides is attributable to the

highly covalent bonds between M (here, P and B) and oxygen in MO_x polyhedral units, which lowers the energy of the oxygen orbitals. This effect decreases the chemical reactivity of the polyanionic compounds with sulfide SSEs and increases the oxidation stability limit significantly. They also computed the reaction energy between each component, including the sulfide SSEs, oxide cathodes, and coating materials, as presented in Figure 10e. As expected, sulfide SSEs show very high reactivity with most of the oxide cathode materials. Interestingly, the reactivity between an oxide coating and a sulfide SSE is similar with that between an oxide cathode and a sulfide SSE (>100 meV/atom). In contrast, the polyanionic coating materials show less reactivity against sulfide SSEs. Similarly, Liu et al. explored the fluorides for cathode coatings using high-throughput computational screening [117]. By screening the phase stability, electrochemical stability, chemical stability, and Li-ion conductivity, they identified Li_2MF_6 (M = Si, Ge, Zr, Ti) compounds as good coating materials. However, their work did not aim for ASSB applications; thus, they did not include the chemical reactivity between SSEs and coating materials, which merit investigation.

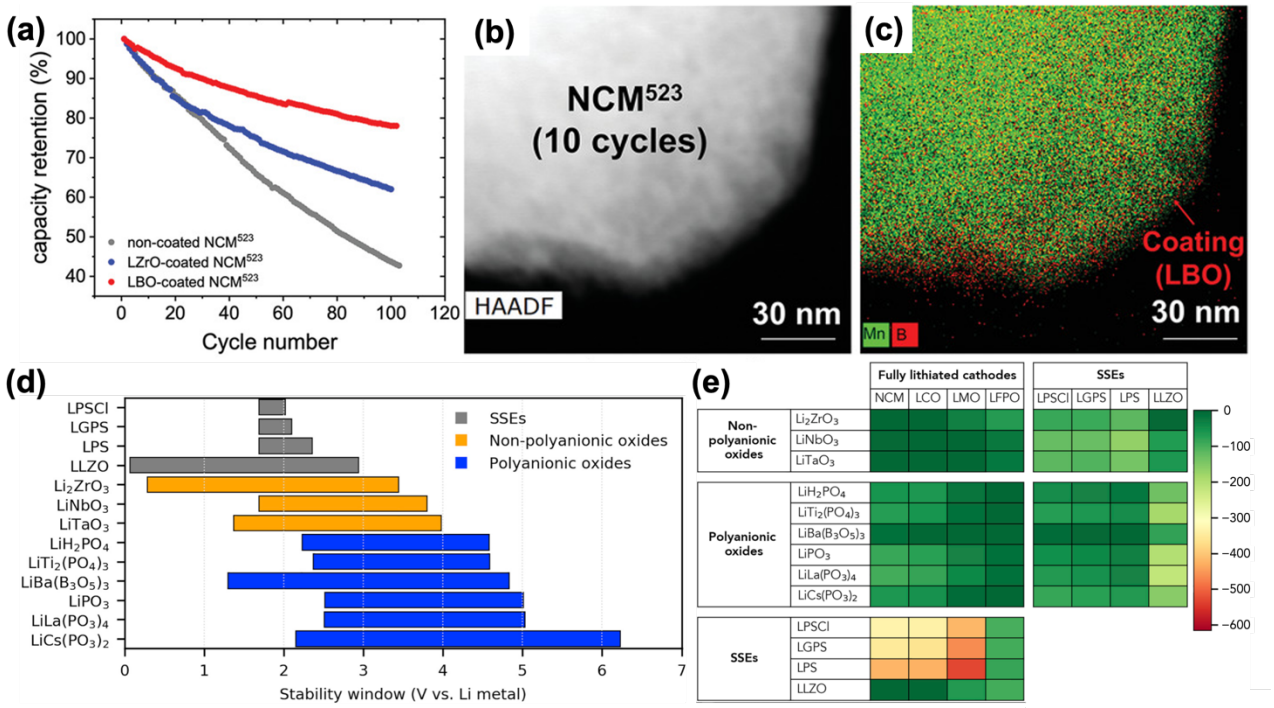

Figure 10. (**a**) Capacity retention on electrochemical cycling of full cells with different coating materials on NCM^{523} cathodes. (**b**) HAADF-STEM image and (**c**) elemental mapping of LZrO-coated sample after 1st cycle, showing aggregation of the decomposition product. Figure a–c are adopted from reference [116] with permission. (**d**) Electrochemical stability windows of common Li-ion conductors. (**e**) Reaction energies ΔE_{rxt} at various interfaces of fully lithiated cathode/SSE, fully lithiated cathode/coating, and coating/SSE in meV/atom. Figure d,e are reprinted from reference [115]. Copyright 2019, with permission from Elsevier.

4. Perspectives and Outlooks

The promise of ASSBs arises from the high safety and use of energy-dense Li-metal anodes. At a very early stage, it was expected that 'hard' and 'non-flammable' SSEs could prevent the dendritic growth of 'soft' Li metals. However, many studies have since demonstrated that Li metals can still penetrate SSEs at relatively high current rates [52,55,118,119]. One simple way to suppress Li dendrite growth is to ensure good contact between the SSE and electrode in order to increase the effective contact area, thereby reducing the effective current. Relatively high stacking pressure can ensure contact between the Li metal and SSE and suppress Li dendrite growth, as demonstrated by Bruce's group [89]. However, too high of a stacking pressure can lead to Li extrusion and thereby Li dendrite penetration through the micropores of the SSE [91,93]. Another strategy is to form a lithiophilic interphase that ensures contact between the Li metal and SSE [90]. This strategy has been widely studied with some successes shown not only in sulfide but also in oxide SSEs [120–123]. However, it is vital to better understand Li-dendrite growth mechanisms. Although there are some plausible explanations, as discussed in Section 3.2, the mechanism is not yet fully understood. We do not expect that a single theory can explain everything but suspect that instead the origin of Li-dendrite formation could depend on the properties of SSEs.

There have been significant efforts to understand SEI formation on both cathodes and anodes since the chemical evolution of SEI plays a critical role in determining the electrochemical properties of ASSBs [71,72,74,99,101,103]. However, our current understanding is still limited, including with respect to the thickness of the interphases and the nature of their microstructures. This lack of knowledge can be mainly attributed to the buried nature inside the solid-state bulk cell, which is thus not readily accessible using most conventional analysis techniques. Further, the extreme reactivity of the Li metal, sulfide SSE, and interphases to moisture, oxygen, and even the electron beam are other important challenges for their characterization. Such high reactivity requires air-tight sample preparation and transfer capabilities for studying buried interfaces since typical sample handling can damage these highly reactive materials. In addition, due to vulnerability to the e-beam, the sample can be damaged during the electron microscopy analyses. Thus, most previous works have been limited to low magnification to minimize the electron-beam dose rate to the sample. However, owing to recent developments of electron microscopy technology, such as a multi-capable TEM sample holders (e.g., offering both cryo and air-tight transfer capabilities in a single holder), high-sensitive electron detectors, etc., it is expected to play a major role soon in investigations of the morphological/structural/chemical properties of the interphase.

Although several works have proposed coating materials that can stabilize the interface between the SSE and cathode active materials [115–117], another critical issue remains, namely the oxidation of the SSE at the interfaces with the conductive additive (e.g., carbon) and current collector (since an SSE is subject to the full cathode potential at such interfaces). Using a low carbon additive content would reduce such oxidation of the SSE. However, a better strategy is required. One alternative could be a dual coating method that uses carbon

nanowire or nano-mesh with uniform cathode active material coating and then SSE coating. This structure will be able to separate electron and ion pathways. Another strategy is to form a passivating interface between a sulfide SSE and carbon.

5. Summary

Sulfide SSEs have attracted significant interest as a key component to realize ASSBs due to their high ionic conductivity and deformability. However, there are remaining challenges. Herein, we provided an overview of the major challenges in interfaces and interphases formed in sulfide SSE systems and the recent progress that has been made in understanding such interface and interphase formation. Then, efforts to address interface and interphase issues in sulfide SSEs were introduced, including several strategies to stabilize the interface or form passivating interphase. Finally, we provided our perspectives on future research directions, with the hope that this review will help guide potential efforts for developing long-lasting and fast-charging solid-state batteries.

Author Contributions: Writing, Y.-W.B. and H.K.; Visualization, Y.-W.B.; Supervision, H.K. Both authors have read and agreed to the published version of the manuscript.

Funding: This work was supported by the Laboratory Directed Research and Development Program of Lawrence Berkeley National Laboratory under U.S. Department of Energy Contract No. DE-AC02-05CH11231.

Data Availability Statement: The data presented in this study are available on request from the corresponding author.

Conflicts of Interest: The authors declare no conflicts of interest.

References

1. Whittingham, M.S. Electrical Energy Storage and Intercalation Chemistry. *Science* **1976**, *192*, 1126–1127, doi:10.1126/science.192.4244.1126.
2. Nagaura, T. A lithium ion battery. *Proceedings of the 5th International Seminar on lithium battery technology and applications*, Deerfield Beach, FL, USA, 5–7 March 1990.
3. Xu, K. Nonaqueous Liquid Electrolytes for Lithium-Based Rechargeable Batteries. *Chem. Rev.* **2004**, *104*, 4303–4418, doi:10.1021/cr030203g.
4. Bruce, P.G. Energy storage beyond the horizon: Rechargeable lithium batteries. *Solid State Ion.* **2008**, *179*, 752–760, doi:10.1016/j.ssi.2008.01.095.
5. Thackeray, M.M.; Wolverton, C.; Isaacs, E.D. Electrical energy storage for transportation—approaching the limits of, and going beyond, lithium-ion batteries. *Energy Environ. Sci.* **2012**, *5*, 7854, doi:10.1039/c2ee21892e.
6. U.S. DRIVE *Electrochemical Energy Storage Technical Team Roadmap*; US Department of Energy: Washington, DC, USA, 2013.

7. Li, C.; Negnevitsky, M.; Wang, X.; Yue, W.L.; Zou, X. Multi-criteria analysis of policies for implementing clean energy vehicles in China. *Energy Policy* **2019**, *129*, 826–840, doi:10.1016/j.enpol.2019.03.002.
8. Takehiko, N. *The Japanese Policy and NEDO Activity for Future Mobility*; Representative office in Europe, New Energy and Industrial Technology Development Organization (NEDO), Paris, France, 2017.
9. Harris, S.J. Unlocking a Secret Stash of Energy. *Joule* **2020**, *4*, 1155–1157, doi:10.1016/j.joule.2020.05.019.
10. Xiao, Y.; Wang, Y.; Bo, S.-H.; Kim, J.C.; Miara, L.J.; Ceder, G. Understanding interface stability in solid-state batteries. *Nat. Rev. Mater.* **2020**, *5*, 105–126, doi:10.1038/s41578-019-0157-5.
11. Tian, Y.; Zeng, G.; Rutt, A.; Shi, T.; Kim, H.; Wang, J.; Koettgen, J.; Sun, Y.; Ouyang, B.; Chen, T.; et al. Promises and Challenges of Next-Generation "Beyond Li-ion" Batteries for Electric Vehicles and Grid Decarbonization. *Chem. Rev.* **2021**, *121*, 1623–1669, doi:10.1021/acs.chemrev.0c00767.
12. Appetecchi, G.B.; Shin, J.H.; Alessandrini, F.; Passerini, S. 0.6Ah Li/V_2O_5 battery prototypes based on solvent-free PEO–$LiN(SO_2CF_2CF_3)_2$ polymer electrolytes. *J. Power Sources* **2005**, *143*, 236–242, doi:10.1016/j.jpowsour.2004.11.039.
13. Seino, Y.; Takada, K.; Kim, B.-C.; Zhang, L.; Ohta, N.; Wada, H.; Osada, M.; Sasaki, T. Synthesis of phosphorous sulfide solid electrolyte and all-solid-state lithium batteries with graphite electrode. *Solid State Ion.* **2005**, *176*, 2389–2393, doi:10.1016/j.ssi.2005.03.026.
14. Monroe, C.; Newman, J. The impact of elastic deformation on deposition kinetics at lithium/polymer interfaces. *J. Electrochem. Soc.* **2005**, *152*, A396–A404.
15. Baba, M.; Kumagai, N.; Fujita, H.; Ohta, K.; Nishidate, K.; Komaba, S.; Kaplan, B.; Groult, H.; Devilliers, D. Multi-layered Li-ion rechargeable batteries for a high-voltage and high-current solid-state power source. *J. Power Sources* **2003**, *119*, 914–917, doi:10.1016/S0378-7753(03)00223-4.
16. Sato, T.; Morinaga, T.; Marukane, S.; Narutomi, T.; Igarashi, T.; Kawano, Y.; Ohno, K.; Fukuda, T.; Tsujii, Y. Novel Solid-State Polymer Electrolyte of Colloidal Crystal Decorated with Ionic-Liquid Polymer Brush. *Adv. Mater.* **2011**, *23*, 4868–4872, doi:10.1002/adma.201101983.
17. Kamaya, N.; Homma, K.; Yamakawa, Y.; Hirayama, M.; Kanno, R.; Yonemura, M.; Kamiyama, T.; Kato, Y.; Hama, S.; Kawamoto, K.; et al. A lithium superionic conductor. *Nat. Mater.* **2011**, *10*, 682–686, doi:10.1038/nmat3066.
18. Tatsumisago, M.; Nagao, M.; Hayashi, A. Recent development of sulfide solid electrolytes and interfacial modification for all-solid-state rechargeable lithium batteries. *J. Asian Ceram. Soc.* **2013**, *1*, 17–25, doi:10.1016/j.jascer.2013.03.005.
19. Richards, W.D.; Miara, L.J.; Wang, Y.; Kim, J.C.; Ceder, G. Interface Stability in Solid-State Batteries. *Chem. Mater.* **2016**, *28*, 266–273, doi:10.1021/acs.chemmater.5b04082.
20. Ma, Z.; Xue, H.-G.; Guo, S.-P. Recent achievements on sulfide-type solid electrolytes: Crystal structures and electrochemical performance. *J. Mater. Sci.* **2018**, *53*, 3927–3938, doi:10.1007/s10853-017-1827-6.
21. Chen, S.; Xie, D.; Liu, G.; Mwizerwa, J.P.; Zhang, Q.; Zhao, Y.; Xu, X.; Yao, X. Sulfide Solid Electrolytes for All-Solid-State Lithium Batteries: Structure, Conductivity, Stability and Application. *Energy Storage Mater.* **2018**, *14*, 58–74, doi:10.1016/j.ensm.2018.02.020.

22. Reddy, M.V.; Julien, C.M.; Mauger, A.; Zaghib, K. Sulfide and Oxide Inorganic Solid Electrolytes for All-Solid-State Li Batteries: A Review. *Nanomaterials* **2020**, 10, 1606, doi:10.3390/nano10081606.
23. Kudu, Ö.U.; Famprikis, T.; Fleutot, B.; Braida, M.-D.; Mercier, T.L.; Islam, M.S.; Masquelier, C. A review of structural properties and synthesis methods of solid electrolyte materials in the $Li_2S-P_2S_5$ binary system. *J. Power Sources* **2018**, *407*, 31–43, doi:10.1016/j.jpowsour.2018.10.037.
24. Kato, Y.; Hori, S.; Saito, T.; Suzuki, K.; Hirayama, M.; Mitsui, A.; Yonemura, M.; Iba, H.; Kanno, R. High-power all-solid-state batteries using sulfide superionic conductors. *Nat. Energy* **2016**, *1*, 16030, doi:10.1038/nenergy.2016.30.
25. Kwon, O.; Hirayama, M.; Suzuki, K.; Kato, Y.; Saito, T.; Yonemura, M.; Kamiyama, T.; Kanno, R. Synthesis, structure, and conduction mechanism of the lithium superionic conductor $Li_{10+\delta}Ge_{1+\delta}P_{2-\delta}S_{12}$. *J. Mater. Chem. A* **2014**, *3*, 438–446, doi:10.1039/c4ta05231e.
26. Sun, Y.; Suzuki, K.; Hori, S.; Hirayama, M.; Kanno, R. Superionic Conductors: $Li_{10+\delta}[Sn_ySi_{1-y}]_{1+\delta}P_{2-\delta}S_{12}$ with a $Li_{10}GeP_2S_{12}$-type Structure in the Li_3PS_4-Li_4SnS_4-Li_4SiS_4 Quasi-ternary System. *Chem. Mater.* **2017**, *29*, 5858–5864, doi:10.1021/acs.chemmater.7b00886.
27. Hori, S.; Suzuki, K.; Hirayama, M.; Kato, Y.; Saito, T.; Yonemura, M.; Kanno, R. Synthesis, structure, and ionic conductivity of solid solution, $Li_{10+\delta}M_{1+\delta}P_{2-\delta}S_{12}$ (M = Si, Sn). *Faraday Discuss.* **2014**, *176*, 83–94, doi:10.1039/c4fd00143e.
28. Seino, Y.; Ota, T.; Takada, K.; Hayashi, A.; Tatsumisago, M. A sulphide lithium super ion conductor is superior to liquid ion conductors for use in rechargeable batteries. *Energy Environ. Sci.* **2013**, 7, 627–631, doi:10.1039/c3ee41655k.
29. Mizuno, F.; Hayashi, A.; Tadanaga, K.; Tatsumisago, M. New, Highly Ion-Conductive Crystals Precipitated from $Li_2S–P_2S_5$ Glasses. *Adv. Mater.* **2005**, *17*, 918–921, doi:10.1002/adma.200401286.
30. Homann, G.; Meister, P.; Stolz, L.; Brinkmann, J.P.; Kulisch, J.; Adermann, T.; Winter, M.; Kasnatscheew, J. High-Voltage All-Solid-State Lithium Battery with Sulfide-Based Electrolyte: Challenges for the Construction of a Bipolar Multicell Stack and How to Overcome Them. *ACS Appl. Energy Mater.* **2020**, *3*, 3162–3168, doi:10.1021/acsaem.0c00041.
31. Minami, K.; Mizuno, F.; Hayashi, A.; Tatsumisago, M. Lithium ion conductivity of the $Li_2S–P_2S_5$ glass-based electrolytes prepared by the melt quenching method. *Solid State Ion.* **2007**, *178*, 837–841, doi:10.1016/j.ssi.2007.03.001.
32. Mizuno, F.; Ohtomo, T.; Hayashi, A.; Tadanaga, K.; Minami, T.; Tatsumisago, M. Structure and Ionic Conductivity of Li_2S-P_2S_5-P_2O_5 Glasses and Glass-Ceramics Prepared by Mechanical Milling. *J. Ceram. Soc. Jpn. Suppl.* **2004**, *112*, S709–S712, doi:10.14852/jcersjsuppl.112.0.S709.0.
33. Tan, D.H.S.; Banerjee, A.; Deng, Z.; Wu, E.A.; Nguyen, H.; Doux, J.-M.; Wang, X.; Cheng, J.-h.; Ong, S.P.; Meng, Y.S.; et al. Enabling Thin and Flexible Solid-State Composite Electrolytes by the Scalable Solution Process. *ACS Appl. Energy Mater.* **2019**, *2*, 6542–6550, doi:10.1021/acsaem.9b01111.
34. Liu, Z.; Fu, W.; Payzant, E.A.; Yu, X.; Wu, Z.; Dudney, N.J.; Kiggans, J.; Hong, K.; Rondinone, A.J.; Liang, C. Anomalous High Ionic Conductivity of Nanoporous β-Li_3PS_4. *J. Am. Chem. Soc.* **2013**, *135*, 975–978, doi:10.1021/ja3110895.

35. Kennedy, J.H.; Zhang, Z.; Eckert, H. Ionically conductive sulfide-based lithium glasses. *J. Non-Cryst. Solids* **1990**, *123*, 328–338, doi:10.1016/0022-3093(90)90804-u.
36. Wada, H.; Menetrier, M.; Levasseur, A.; Hagenmuller, P. Preparation and ionic conductivity of new B_2S_3-Li_2S-LiI glasses. *Mater. Res. Bull.* **1983**, *18*, 189–193, doi:10.1016/0025-5408(83)90080-6.
37. Yamauchi, A.; Sakuda, A.; Hayashi, A.; Tatsumisago, M. Preparation and ionic conductivities of (100 − x)(0.75Li_2S·0.25P_2S_5)·xLiBH4 glass electrolytes. *J. Power Sources* **2013**, *244*, 707–710, doi:10.1016/j.jpowsour.2012.12.001.
38. Dietrich, C.; Weber, D.A.; Sedlmaier, S.J.; Indris, S.; Culver, S.P.; Walter, D.; Janek, J.; Zeier, W.G. Lithium ion conductivity in Li_2S–P_2S_5 glasses—Building units and local structure evolution during the crystallization of superionic conductors Li_3PS_4, $Li_7P_3S_{11}$ and $Li_4P_2S_7$. *J. Mater. Chem. A* **2017**, *5*, 18111–18119, doi:10.1039/c7ta06067j.
39. Hayashi, A.; Hama, S.; Minami, T.; Tatsumisago, M. Formation of superionic crystals from mechanically milled Li_2S–P_2S_5 glasses. *Electrochem. Commun.* **2003**, *5*, 111–114, doi:10.1016/s1388-2481(02)00555-6.
40. Marple, M.A.T.; Aitken, B.G.; Kim, S.; Sen, S. Fast Li-Ion Dynamics in Stoichiometric Li_2S–Ga_2Se_3–$GeSe_2$ Glasses. *Chem. Mater.* **2017**, *29*, 8704–8710, doi:10.1021/acs.chemmater.7b02858.
41. Ohno, S.; Bernges, T.; Buchheim, J.; Duchardt, M.; Hatz, A.-K.; Kraft, M.A.; Kwak, H.; Santhosha, A.L.; Liu, Z.; Minafra, N.; et al. How Certain Are the Reported Ionic Conductivities of Thiophosphate-Based Solid Electrolytes? An Interlaboratory Study. *ACS Energy Lett.* **2020**, *5*, 910–915, doi:10.1021/acsenergylett.9b02764.
42. Zhang, Z.; Zhang, L.; Liu, Y.; Yu, C.; Yan, X.; Xu, B.; Wang, L.-m. Synthesis and characterization of argyrodite solid electrolytes for all-solid-state Li-ion batteries. *J. Alloy. Compd.* **2018**, *747*, 227–235, doi:10.1016/j.jallcom.2018.03.027.
43. Zhang, Z.; Zhang, L.; Yan, X.; Wang, H.; Liu, Y.; Yu, C.; Cao, X.; Eijck, L.V.; Wen, B. All-in-one improvement toward Li6PS5Br-Based solid electrolytes triggered by compositional tune. *J. Power Sources* **2019**, *410*, 162–170, doi:10.1016/j.jpowsour.2018.11.016.
44. Rangasamy, E.; Liu, Z.; Gobet, M.; Pilar, K.; Sahu, G.; Zhou, W.; Wu, H.; Greenbaum, S.; Liang, C. An iodide-based $Li_7P_2S_8I$ superionic conductor. *J. Am. Chem. Soc.* **2015**, *137*, 1384–1387, doi:10.1021/ja508723m.
45. Huang, W.; Yoshino, K.; Hori, S.; Suzuki, K.; Yonemura, M.; Hirayama, M.; Kanno, R. Superionic Lithium Conductor with a Cubic Argyrodite-type Structure in the Li–Al–Si–S system. *J. Solid State Chem.* **2018**, *270*, 487–492, doi:10.1016/j.jssc.2018.12.015.
46. Stallworth, P.E.; Fontanella, J.J.; Wintersgill, M.C.; Scheidler, C.D.; Immel, J.J.; Greenbaum, S.G.; Gozdz, A.S. NMR, DSC and high pressure electrical conductivity studies of liquid and hybrid electrolytes. *J. Power Sources* **1999**, *81*, 739–747, doi:10.1016/s0378-7753(99)00144-5.
47. Kanno, R.; Murayama, M. Lithium Ionic Conductor Thio-LISICON: The Li_2S-GeS_2-P_2S_5 System. *J. Electrochem. Soc.* **2001**, *148*, A742, doi:10.1149/1.1379028.
48. Han, F.; Zhu, Y.; He, X.; Mo, Y.; Wang, C. Electrochemical Stability of $Li_{10}GeP_2S_{12}$ and $Li_7La_3Zr_2O_{12}$ Solid Electrolytes. *Adv. Energy Mater.* **2016**, *6*, 1501590, doi:10.1002/aenm.201501590.

49. Dewald, G.F.; Ohno, S.; Kraft, M.A.; Koerver, R.; Till, P.; Vargas-Barbosa, N.M.; Janek, J.; Zeier, W.G. Experimental Assessment of the Practical Oxidative Stability of Lithium Thiophosphate Solid Electrolytes. *Chem. Mater.* **2019**, *31*, 8328–8337, doi:10.1021/acs.chemmater.9b01550.
50. Zhu, Y.; He, X.; Mo, Y. Origin of Outstanding Stability in the Lithium Solid Electrolyte Materials: Insights from Thermodynamic Analyses Based on First-Principles Calculations. *ACS Appl. Mater. Interfaces* **2015**, *7*, 23685–23693, doi:10.1021/acsami.5b07517.
51. Zhu, Y.; He, X.; Mo, Y. First principles study on electrochemical and chemical stability of solid electrolyte–electrode interfaces in all-solid-state Li-ion batteries. *J. Mater. Chem. A* **2016**, *4*, 3253–3266, doi:10.1039/C5TA08574H.
52. Porz, L.; Swamy, T.; Sheldon, B.W.; Rettenwander, D.; Frömling, T.; Thaman, H.L.; Berendts, S.; Uecker, R.; Carter, W.C.; Chiang, Y.-M. Mechanism of Lithium Metal Penetration through Inorganic Solid Electrolytes. *Adv. Energy Mater.* **2017**, *7*, 1701003, doi:10.1002/aenm.201701003.
53. Lewis, J.A.; Cortes, F.J.Q.; Boebinger, M.G.; Tippens, J.; Marchese, T.S.; Kondekar, N.; Liu, X.; Chi, M.; McDowell, M.T. Interphase Morphology between a Solid-State Electrolyte and Lithium Controls Cell Failure. *ACS Energy Lett.* **2019**, *4*, 591–599, doi:10.1021/acsenergylett.9b00093.
54. Kazyak, E.; Garcia-Mendez, R.; LePage, W.S.; Sharafi, A.; Davis, A.L.; Sanchez, A.J.; Chen, K.-H.; Haslam, C.; Sakamoto, J.; Dasgupta, N.P. Li Penetration in Ceramic Solid Electrolytes: Operando Microscopy Analysis of Morphology, Propagation, and Reversibility. *Matter* **2020**, *2*, 1025–1048, doi:10.1016/j.matt.2020.02.008.
55. Ji, X.; Hou, S.; Wang, P.; He, X.; Piao, N.; Chen, J.; Fan, X.; Wang, C. Solid-State Electrolyte Design for Lithium Dendrite Suppression. *Adv. Mater.* **2020**, *32*, 2002741, doi:10.1002/adma.202002741.
56. Takada, K.; Ohta, N.; Zhang, L.; Fukuda, K.; Sakaguchi, I.; Ma, R.; Osada, M.; Sasaki, T. Interfacial modification for high-power solid-state lithium batteries. *Solid State Ion.* **2008**, *179*, 1333–1337, doi:10.1016/j.ssi.2008.02.017.
57. Nagao, M.; Hayashi, A.; Tatsumisago, M. Fabrication of favorable interface between sulfide solid electrolyte and Li metal electrode for bulk-type solid-state Li/S battery. *Electrochem. Commun.* **2012**, *22*, 177–180, doi:10.1016/j.elecom.2012.06.015.
58. Huang, B.; Yao, X.; Huang, Z.; Guan, Y.; Jin, Y.; Xu, X. Li3PO4-doped Li7P3S11 glass-ceramic electrolytes with enhanced lithium ion conductivities and application in all-solid-state batteries. *J. Power Sources* **2015**, *284*, 206–211, doi:10.1016/j.jpowsour.2015.02.160.
59. Yu, C.; Ganapathy, S.; Klerk, N.J.J.d.; Roslon, I.; Eck, E.R.H.v.; Kentgens, A.P.M.; Wagemaker, M. Unravelling Li-Ion Transport from Picoseconds to Seconds: Bulk versus Interfaces in an Argyrodite Li_6PS_5Cl–Li_2S All-Solid-State Li-Ion Battery. *J. Am. Chem. Soc.* **2016**, *138*, 11192–11201, doi:10.1021/jacs.6b05066.
60. Sakuma, M.; Suzuki, K.; Hirayama, M.; Kanno, R. Reactions at the electrode/electrolyte interface of all-solid-state lithium batteries incorporating Li–M (M = Sn, Si) alloy electrodes and sulfide-based solid electrolytes. *Solid State Ion.* **2016**, *285*, 101–105, doi:10.1016/j.ssi.2015.07.010.
61. Bachman, J.C.; Muy, S.; Grimaud, A.; Chang, H.-H.; Pour, N.; Lux, S.F.; Paschos, O.; Maglia, F.; Lupart, S.; Lamp, P.; et al. Inorganic Solid-State Electrolytes for Lithium Batteries: Mechanisms and Properties Governing Ion Conduction. *Chem. Rev.* **2016**, *116*, 140–162, doi:10.1021/acs.chemrev.5b00563.

62. Hayashi, A.; Sakuda, A.; Tatsumisago, M. Development of Sulfide Solid Electrolytes and Interface Formation Processes for Bulk-Type All-Solid-State Li and Na Batteries. *Front. Energy Res.* **2016**, *4*, 25, doi:10.3389/fenrg.2016.00025.
63. Auvergniot, J.; Cassel, A.; Foix, D.; Viallet, V.; Seznec, V.; Dedryvère, R. Redox activity of argyrodite Li6PS5Cl electrolyte in all-solid-state Li-ion battery: An XPS study. *Solid State Ion.* **2017**, *300*, 78–85, doi:10.1016/j.ssi.2016.11.029.
64. Ito, Y.; Otoyama, M.; Hayashi, A.; Ohtomo, T.; Tatsumisago, M. Electrochemical and structural evaluation for bulk-type all-solid-state batteries using Li4GeS4-Li3PS4 electrolyte coating on $LiCoO_2$ particles. *J. Power Sources* **2017**, *360*, 328–335, doi:10.1016/j.jpowsour.2017.05.112.
65. Yu, C.; Ganapathy, S.; Eck, E.R.H.v.; Wang, H.; Basak, S.; Li, Z.; Wagemaker, M. Accessing the bottleneck in all-solid state batteries, lithium-ion transport over the solid-electrolyte-electrode interface. *Nat. Commun.* **2017**, *8*, 1086, doi:10.1038/s41467-017-01187-y.
66. Kato, A.; Kowada, H.; Deguchi, M.; Hotehama, C.; Hayashi, A.; Tatsumisago, M. XPS and SEM analysis between Li/Li3PS4 interface with Au thin film for all-solid-state lithium batteries. *Solid State Ion.* **2018**, *322*, 1–4, doi:10.1016/j.ssi.2018.04.011.
67. Chen, B.; Xu, C.; Wang, H.; Zhou, J. Insights into interfacial stability of Li6PS5Cl solid electrolytes with buffer layers. *Curr. Appl. Phys.* **2018**, *19*, 149–154, doi:10.1016/j.cap.2018.12.003.
68. Wenzel, S.; Leichtweiss, T.; Krüger, D.; Sann, J.; Janek, J. Interphase formation on lithium solid electrolytes—An in situ approach to study interfacial reactions by photoelectron spectroscopy. *Solid State Ion.* **2015**, *278*, 98–105, doi:10.1016/j.ssi.2015.06.001.
69. Wenzel, S.; Leichtweiss, T.; Weber, D.A.; Sann, J.; Zeier, W.G.; Janek, J. Interfacial Reactivity Benchmarking of the Sodium Ion Conductors Na_3PS_4 and Sodium β-Alumina for Protected Sodium Metal Anodes and Sodium All-Solid-State Batteries. *ACS Appl. Mater. Interfaces* **2016**, 8, 28216–28224, doi:10.1021/acsami.6b10119.
70. Wenzel, S.; Weber, D.A.; Leichtweiss, T.; Busche, M.R.; Sann, J.; Janek, J. Interphase formation and degradation of charge transfer kinetics between a lithium metal anode and highly crystalline Li7P3S11 solid electrolyte. *Solid State Ion.* **2016**, *286*, 24–33, doi:10.1016/j.ssi.2015.11.034.
71. Wenzel, S.; Sedlmaier, S.J.; Dietrich, C.; Zeier, W.G.; Janek, J. Interfacial reactivity and interphase growth of argyrodite solid electrolytes at lithium metal electrodes. *Solid State Ion.* **2018**, *318*, 102–112, doi:10.1016/j.ssi.2017.07.005.
72. Wenzel, S.; Randau, S.; Leichtweiß, T.; Weber, D.A.; Sann, J.; Zeier, W.G.; Janek, J.r. Direct Observation of the Interfacial Instability of the Fast Ionic Conductor $Li_{10}GeP_2S_{12}$ at the Lithium Metal Anode. *Chem. Mater.* **2016**, *28*, 2400–2407, doi:10.1021/acs.chemmater.6b00610.
73. Cheng, T.; Merinov, B.V.; Morozov, S.; Goddard, W.A. Quantum Mechanics Reactive Dynamics Study of Solid Li-Electrode/Li_6PS_5Cl-Electrolyte Interface. *ACS Energy Lett.* **2017**, *2*, 1454–1459, doi:10.1021/acsenergylett.7b00319.
74. Wood, K.N.; Steirer, K.X.; Hafner, S.E.; Ban, C.; Santhanagopalan, S.; Lee, S.-H.; Teeter, G. Operando X-ray photoelectron spectroscopy of solid electrolyte interphase formation and evolution in Li_2S-P_2S_5 solid-state electrolytes. *Nat. Commun.* **2018**, *9*, 2490, doi:10.1038/s41467-018-04762-z..

75. Wang, C.; Zhao, Y.; Sun, Q.; Li, X.; Liu, Y.; Liang, J.; Li, X.; Lin, X.; Li, R.; Adair, K.R.; et al. Stabilizing interface between Li10SnP2S12 and Li metal by molecular layer deposition. *Nano Energy* **2018**, *53*, 168–174, doi:10.1016/j.nanoen.2018.08.030.
76. Ye, L.; Li, X. A dynamic stability design strategy for lithium metal solid state batteries. *Nature* **2021**, *593*, 218–222, doi:10.1038/s41586-021-03486-3.
77. Yang, Y.; Han, J.; DeVita, M.; Lee, S.S.; Kim, J.C. Lithium and Chlorine-Rich Preparation of Mechanochemically Activated Antiperovskite Composites for Solid-State Batteries. *Front. Chem.* **2020**, *8*, 562549, doi:10.3389/fchem.2020.562549.
78. Han, F.; Yue, J.; Zhu, X.; Wang, C. Suppressing Li Dendrite Formation in Li_2S-P_2S_5 Solid Electrolyte by LiI Incorporation. *Adv. Energy Mater.* **2018**, *8*, 1703644, doi:10.1002/aenm.201703644.
79. Garcia-Mendez, R.; Mizuno, F.; Zhang, R.; Arthur, T.S.; Sakamoto, J. Effect of Processing Conditions of 75Li2S-25P2S5 Solid Electrolyte on its DC Electrochemical Behavior. *Electrochim. Acta* **2017**, *237*, 144–151, doi:10.1016/j.electacta.2017.03.200.
80. Liu, G.; Weng, W.; Zhang, Z.; Wu, L.; Yang, J.; Yao, X. Densified Li6PS5Cl Nanorods with High Ionic Conductivity and Improved Critical Current Density for All-Solid-State Lithium Batteries. *Nano Lett.* **2020**, *20*, 6660–6665, doi:10.1021/acs.nanolett.0c02489.
81. Lee, Y.; Jeong, J.; Lim, H.-D.; Kim, S.-O.; Jung, H.-G.; Chung, K.Y.; Yu, S. Superionic Si-Substituted Lithium Argyrodite Sulfide Electrolyte $Li_{6+x}Sb_{1-x}Si_xS_5I$ for All-Solid-State Batteries. *ACS Sustain. Chem. Eng.* **2021**, *9*, 120–128, doi:10.1021/acssuschemeng.0c05549.
82. Qian, J.; Henderson, W.A.; Xu, W.; Bhattacharya, P.; Engelhard, M.; Borodin, O.; Zhang, J.-G. High rate and stable cycling of lithium metal anode. *Nat. Commun.* **2015**, *6*, 6362, doi:10.1038/ncomms7362.
83. Otoyama, M.; Suyama, M.; Hotehama, C.; Kowada, H.; Takeda, Y.; Ito, K.; Sakuda, A.; Tatsumisago, M.; Hayashi, A. Visualization and Control of Chemically Induced Crack Formation in All-Solid-State Lithium-Metal Batteries with Sulfide Electrolyte. *ACS Appl. Mater. Interfaces* **2021**, 13*,* 5000–5007, doi:10.1021/acsami.0c18314.
84. Ning, Z.; Jolly, D.S.; Li, G.; De Meyere, R.; Pu, S.D.; Chen, Y.; Kasemchainan, J.; Ihli, J.; Gong, C.; Liu, B.; et al. Visualizing plating-induced cracking in lithium-anode solid-electrolyte cells. *Nat. Mater.* **2021**, *322*, 1–4, doi:10.1038/s41563-021-00967-8.
85. Han, F.; Westover, A.S.; Yue, J.; Fan, X.; Wang, F.; Chi, M.; Leonard, D.N.; Dudney, N.J.; Wang, H.; Wang, C. High electronic conductivity as the origin of lithium dendrite formation within solid electrolytes. *Nat. Energy* **2019**, *4*, 187–196, doi:10.1038/s41560-018-0312-z.
86. Li, J.; Dudney, N.J.; Nanda, J.; Liang, C. Artificial Solid Electrolyte Interphase To Address the Electrochemical Degradation of Silicon Electrodes. *ACS Appl. Mater. Interfaces* **2014**, *6*, 10083–10088, doi:10.1021/am5009419.
87. Le Van-Jodin, L.; Ducroquet, F.; Sabary, F.; Chevalier, I. Dielectric properties, conductivity and Li+ ion motion in LiPON thin films. *Solid State Ion.* **2013**, *253*, 151–156, doi:10.1016/j.ssi.2013.09.031.
88. Su, Y.; Falgenhauer, J.; Polity, A.; Leichtweiß, T.; Kronenberger, A.; Obel, J.; Zhou, S.; Schlettwein, D.; Janek, J.; Meyer, B.K. LiPON thin films with high nitrogen content for application in lithium batteries and electrochromic devices prepared by RF magnetron sputtering. *Solid State Ion.* **2015**, *282*, 63–69, doi:10.1016/j.ssi.2015.09.022.

89. Kasemchainan, J.; Zekoll, S.; Jolly, D.S.; Ning, Z.; Hartley, G.O.; Marrow, J.; Bruce, P.G. Critical stripping current leads to dendrite formation on plating in lithium anode solid electrolyte cells. *Nat. Mater.* **2019**, *18*, 1105–1111, doi:10.1038/s41563-019-0438-9.
90. Yang, C.-T.; Qi, Y. Maintaining a Flat Li Surface during the Li Stripping Process via Interface Design. *Chem. Mater.* **2021**, *33*, 2814–2823, doi:10.1021/acs.chemmater.0c04814.
91. Doux, J.-M.; Nguyen, H.; Tan, D.H.S.; Banerjee, A.; Wang, X.; Wu, E.A.; Jo, C.; Yang, H.; Meng, Y.S. Stack Pressure Considerations for Room-Temperature All-Solid-State Lithium Metal Batteries. *Adv. Energy Mater.* **2020**, *10*, 1903253, doi:10.1002/aenm.201903253.
92. Hänsel, C.; Kumar, P.V.; Kundu, D. Stack Pressure Effect in Li_3PS_4 and Na_3PS_4 Based Alkali Metal Solid-State Cells: The Dramatic Implication of Interlayer Growth. *Chem. Mater.* **2020**, *32*, 10501–10510, doi:10.1021/acs.chemmater.0c03444.
93. Hänsel, C.; Kundu, D. The Stack Pressure Dilemma in Sulfide Electrolyte Based Li Metal Solid-State Batteries: A Case Study with Li_6PS_5Cl Solid Electrolyte. *Adv. Mater. Interfaces* **2021**, 2100206, doi:10.1002/admi.202100206.
94. Wang, Y.; Liu, T.; Kumar, J. Effect of Pressure on Lithium Metal Deposition and Stripping against Sulfide-Based Solid Electrolytes. *ACS Appl. Mater. Interfaces* **2020**, *12*, 34771–34776, doi:10.1021/acsami.0c06201.
95. Yoon, K.; Kim, J.-J.; Seong, W.M.; Lee, M.H.; Kang, K. Investigation on the interface between $Li_{10}GeP_2S_{12}$ electrolyte and carbon conductive agents in all-solid-state lithium battery. *Sci. Rep.* **2018**, *8*, 8066, doi:10.1038/s41598-018-26101-4.
96. Zhang, W.; Leichtweiß, T.; Culver, S.P.; Koerver, R.; Das, D.; Weber, D.A.; Zeier, W.G.; Janek, J. The Detrimental Effects of Carbon Additives in $Li_{10}GeP_2S_{12}$-Based Solid-State Batteries. *ACS Appl. Mater. Interfaces* **2017**, *9*, 35888–35896, doi:10.1021/acsami.7b11530.
97. Koerver, R.; Walther, F.; Aygün, I.; Sann, J.; Dietrich, C.; Zeier, W.G.; Janek, J. Redox-active cathode interphases in solid-state batteries. *J. Mater. Chem. A* **2017**, *5*, 22750–22760, doi:10.1039/C7TA07641J.
98. Oh, G.; Hirayama, M.; Kwon, O.; Suzuki, K.; Kanno, R. Bulk-Type All Solid-State Batteries with 5 V Class $LiNi_{0.5}Mn_{1.5}O_4$ Cathode and $Li_{10}GeP_2S_{12}$ Solid Electrolyte. *Chem. Mater.* **2016**, *28*, 2634–2640, doi:10.1021/acs.chemmater.5b04940.
99. Sakuda, A.; Hayashi, A.; Tatsumisago, M. Interfacial Observation between $LiCoO_2$ Electrode and $Li_2S-P_2S_5$ Solid Electrolytes of All-Solid-State Lithium Secondary Batteries Using Transmission Electron Microscopy. *Chem. Mater.* **2010**, *22*, 949–956, doi:10.1021/cm901819c.
100. Zhang, J.; Zheng, C.; Li, L.; Xia, Y.; Huang, H.; Gan, Y.; Liang, C.; He, X.; Tao, X.; Zhang, W. Unraveling the Intra and Intercycle Interfacial Evolution of Li_6PS_5Cl-Based All-Solid-State Lithium Batteries. *Adv. Energy Mater.* **2020**, *10*, 1903311, doi:10.1002/aenm.201903311.
101. Walther, F.; Koerver, R.; Fuchs, T.; Ohno, S.; Sann, J.; Rohnke, M.; Zeier, W.G.; Janek, J.r. Visualization of the Interfacial Decomposition of Composite Cathodes in Argyrodite-Based All-Solid-State Batteries Using Time-of-Flight Secondary-Ion Mass Spectrometry. *Chem. Mater.* **2019**, *31*, 3745–3755, doi:10.1021/acs.chemmater.9b00770.

102. Visbal, H.; Aihara, Y.; Ito, S.; Watanabe, T.; Park, Y.; Doo, S. The effect of diamond-like carbon coating on $LiNi_{0.8}Co_{0.15}Al_{0.05}O_2$ particles for all solid-state lithium-ion batteries based on Li2S–P2S5 glass-ceramics. *J. Power Sources* **2016**, *314*, 85–92, doi:10.1016/j.jpowsour.2016.02.088.
103. Auvergniot, J.; Cassel, A.; Ledeuil, J.-B.; Viallet, V.; Seznec, V.; Dedryvère, R. Interface Stability of Argyrodite Li_6PS_5Cl toward $LiCoO_2$, $LiNi_{1/3}Co_{1/3}Mn_{1/3}O_2$, and $LiMn_2O_4$ in Bulk All-Solid-State Batteries. *Chem. Mater.* **2017**, *29*, 3883–3890, doi:10.1021/acs.chemmater.6b04990.
104. Ye, L.; Fitzhugh, W.; Gil-González, E.; Wang, Y.; Su, Y.; Su, H.; Qiao, T.; Ma, L.; Zhou, H.; Hu, E.; et al. Toward Higher Voltage Solid-State Batteries by Metastability and Kinetic Stability Design. *Adv. Energy Mater.* **2020**, *10*, 2001569, doi:10.1002/aenm.202001569.
105. Fitzhugh, W.; Ye, L.; Li, X. The effects of mechanical constriction on the operation of sulfide based solid-state batteries. *J. Mater. Chem. A* **2019**, *7*, 23604–23627, doi:10.1039/C9TA05248H.
106. Culver, S.P.; Koerver, R.; Zeier, W.G.; Janek, J. On the Functionality of Coatings for Cathode Active Materials in Thiophosphate-Based All-Solid-State Batteries. *Adv. Energy Mater.* **2019**, *9*, 1900626, doi:10.1002/aenm.201900626.
107. Ohta, N.; Takada, K.; Sakaguchi, I.; Zhang, L.; Ma, R.; Fukuda, K.; Osada, M.; Sasaki, T. $LiNbO_3$-coated $LiCoO_2$ as cathode material for all solid-state lithium secondary batteries. *Electrochem. Commun.* **2007**, *9*, 1486–1490, doi:10.1016/j.elecom.2007.02.008.
108. Ito, S.; Fujiki, S.; Yamada, T.; Aihara, Y.; Park, Y.; Kim, T.Y.; Baek, S.-W.; Lee, J.-M.; Doo, S.; Machida, N. A rocking chair type all-solid-state lithium ion battery adopting Li_2O–ZrO_2 coated $LiNi_{0.8}Co_{0.15}Al_{0.05}O_2$ and a sulfide based electrolyte. *J. Power Sources* **2014**, *248*, 943–950, doi:10.1016/j.jpowsour.2013.10.005.
109. Lee, J.W.; Park, Y.J. Enhanced Cathode/Sulfide Electrolyte Interface Stability Using an Li_2ZrO_3 Coating for All-Solid-State Batteries. *J. Electrochem. Sci. Technol* **2018**, *9*, 176–183, doi:10.5229/JECST.2018.9.3.176.
110. Ohta, N.; Takada, K.; Zhang, L.; Ma, R.; Osada, M.; Sasaki, T. Enhancement of the High-Rate Capability of Solid-State Lithium Batteries by Nanoscale Interfacial Modification. *Adv. Mater.* **2006**, *18*, 2226–2229, doi:10.1002/adma.200502604.
111. Kitaura, H.; Hayashi, A.; Tadanaga, K.; Tatsumisago, M. Improvement of electrochemical performance of all-solid-state lithium secondary batteries by surface modification of $LiMn_2O_4$ positive electrode. *Solid State Ion.* **2011**, *192*, 304–307, doi:10.1016/j.ssi.2010.08.019.
112. Okada, K.; Machida, N.; Naito, M.; Shigematsu, T.; Ito, S.; Fujiki, S.; Nakano, M.; Aihara, Y. Preparation and electrochemical properties of $LiAlO_2$-coated $Li(Ni_{1/3}Mn_{1/3}Co_{1/3})O_2$ for all-solid-state batteries. *Solid State Ion.* **2014**, *255*, 120–127, doi:10.1016/j.ssi.2013.12.019.
113. Wang, C.-W.; Ren, F.-C.; Zhou, Y.; Yan, P.-F.; Zhou, X.-D.; Zhang, S.-J.; Liu, W.; Zhang, W.-D.; Zou, M.-H.; Zeng, L.-Y.; et al. Engineering the interface between $LiCoO_2$ and $Li_{10}GeP_2S_{12}$ solid electrolytes with an ultrathin Li2CoTi3O8 interlayer to boost the performance of all-solid-state batteries. *Energy Environ. Sci.* **2021**, *14*, 437–450, doi:10.1039/D0EE03212C.
114. Walther, F.; Randau, S.; Schneider, Y.; Sann, J.; Rohnke, M.; Richter, F.H.; Zeier, W.G.; Janek, J. Influence of Carbon Additives on the Decomposition Pathways in Cathodes of Lithium Thiophosphate-Based All-Solid-State Batteries. *Chem. Mater.* **2020**, 32, 6123–6136, doi:10.1021/acs.chemmater.0c01825.

115. Xiao, Y.; Miara, L.J.; Wang, Y.; Ceder, G. Computational Screening of Cathode Coatings for Solid-State Batteries. *Joule* **2019**, *3*, 1252–1275, doi:10.1016/j.joule.2019.02.006.
116. Zhang, Y.-Q.; Tian, Y.; Xiao, Y.; Miara, L.J.; Aihara, Y.; Tsujimura, T.; Shi, T.; Scott, M.C.; Ceder, G. Direct Visualization of the Interfacial Degradation of Cathode Coatings in Solid State Batteries: A Combined Experimental and Computational Study. *Adv. Energy Mater.* **2020**, *10*, 1903778, doi:10.1002/aenm.201903778.
117. Liu, B.; Wang, D.; Avdeev, M.; Shi, S.; Yang, J.; Zhang, W. High-Throughput Computational Screening of Li-Containing Fluorides for Battery Cathode Coatings. *ACS Sustain. Chem. Eng.* **2020**, 8, 948–957, doi:10.1021/acssuschemeng.9b05557.
118. Liu, X.; Garcia-Mendez, R.; Lupini, A.R.; Cheng, Y.; Hood, Z.D.; Han, F.; Sharafi, A.; Idrobo, J.C.; Dudney, N.J.; Wang, C.; et al. Local electronic structure variation resulting in Li 'filament' formation within solid electrolytes. *Nat. Mater.* **2021**, 1–6, doi:10.1038/s41563-021-01019-x.
119. Swamy, T.; Park, R.; Sheldon, B.W.; Rettenwander, D.; Porz, L.; Berendts, S.; Uecker, R.; Carter, W.C.; Chiang, Y.-M. Lithium Metal Penetration Induced by Electrodeposition through Solid Electrolytes: Example in Single-Crystal $Li_6La_3ZrTaO_{12}$ Garnet. *J. Electrochem. Soc.* **2018**, *165*, A3648–A3655, doi:10.1149/2.1391814jes.
120. Feng, W.; Dong, X.; Lai, Z.; Zhang, X.; Wang, Y.; Wang, C.; Luo, J.; Xia, Y. Building an Interfacial Framework: Li/Garnet Interface Stabilization through a Cu_6Sn_5 Layer. *ACS Energy Lett.* **2019**, *4*, 1725–1731, doi:10.1021/acsenergylett.9b01158.
121. Kim, K.J.; Rupp, J.L.M. All ceramic cathode composite design and manufacturing towards low interfacial resistance for garnet-based solid-state lithium batteries. *Energy Environ. Sci.* **2020**, *13*, 4930–4945, doi:10.1039/d0ee02062a.
122. Pervez, S.A.; Kim, G.; Vinayan, B.P.; Cambaz, M.A.; Kuenzel, M.; Hekmatfar, M.; Fichtner, M.; Passerini, S. Overcoming the Interfacial Limitations Imposed by the Solid–Solid Interface in Solid-State Batteries Using Ionic Liquid-Based Interlayers. *Small* **2020**, *16*, 2000279, doi:10.1002/smll.202000279.
123. Kim, K.J.; Balaish, M.; Wadaguchi, M.; Kong, L.; Rupp, J.L.M. Solid-State Li–Metal Batteries: Challenges and Horizons of Oxide and Sulfide Solid Electrolytes and Their Interfaces. *Adv. Energy Mater.* **2021**, *11*, 2002689, doi:10.1002/aenm.202002689.